

# **$\alpha$ -Synuclein interacts with the switch region of Rab8a in a Ser129 phosphorylation-dependent manner**

Guowei Yin<sup>1,♦</sup>, Tomas Lopes da Fonseca<sup>4,5,♦</sup>, Sibylle E. Eisbach<sup>4,5</sup>, Ane Martín Anduaga<sup>9</sup>, Carlo Breda<sup>9</sup>, Maria L. Orcellet<sup>6</sup>, Éva M. Szegő<sup>4,5</sup>, Patricia Guerreiro<sup>4,5</sup>, Diana Lazaro<sup>4,5</sup>, Gerhard H. Braus<sup>3,5</sup>, Claudio O. Fernandez<sup>6</sup>, Christian Griesinger<sup>1</sup>, Stefan Becker<sup>1</sup>, Roger S. Goody<sup>8</sup>, Aymelt Itzen<sup>7,8</sup>, Flaviano Giorgini<sup>9</sup>, Tiago F. Outeiro<sup>4,5,\*</sup> and Markus Zweckstetter<sup>1,2,5,\*</sup>

<sup>1</sup>Department of NMR-based Structural Biology, Max Planck Institute for Biophysical Chemistry, Göttingen, Germany

<sup>2</sup>German Center for Neurodegenerative Diseases (DZNE), D-37077, Göttingen, Germany <sup>3</sup>Dept. Molecular Microbiology and Genetics, Institute of Microbiology & Genetics, Georg-August-Universität Göttingen, D-37077, Göttingen, Germany

<sup>4</sup>Department of Neurodegeneration and Restorative Research, University Medicine Göttingen, Göttingen, Germany <sup>5</sup>DFG

Research Center Nanoscale Microscopy and Molecular Physiology of the Brain (CNMPB), Göttingen, Germany <sup>6</sup>Max

Planck for Structural Biology, Chemistry and Molecular Biophysics of Rosario (MPLbioR), Universidad Nacional de

Rosario, IBR-CONICET, Ocampo y Esmeralda, 2000 Rosario, Argentina, <sup>7</sup>Center for Integrated Protein Science Munich,

Chemistry Department, Technische Universität München, Lichtenbergstr. 4, 85748 Garching, Germany,

<sup>8</sup>Max-Planck-Institute of Molecular Physiology, Department of Physical Biochemistry, Dortmund 44227,

Germany, <sup>9</sup>Department of Genetics, University of Leicester, Leicester, LE1 7RH, UK.

♦ These authors contributed equally.

Corresponding authors

markus.zweckstetter@dzne.de

tiago.outeiro@med.uni-goettingen.de

**Key words:**  $\alpha$ -synuclein/aggregation/Parkinson disease/phosphorylation/Rab GTPase

## ABSTRACT

Alpha-Synuclein ( $\alpha$ S) misfolding is associated with Parkinson's disease (PD) but little is known about the mechanisms underlying  $\alpha$ S toxicity. Increasing evidence suggests that defects in membrane transport play an important role in neuronal dysfunction. Here we demonstrate that the GTPase Rab8a interacts with  $\alpha$ S in rodent brain. NMR spectroscopy reveals that the C-terminus of  $\alpha$ S binds to the functionally important switch region as well as the C-terminal tail of Rab8a. In line with a direct Rab8a/ $\alpha$ S interaction, Rab8a enhanced  $\alpha$ S aggregation and reduced  $\alpha$ S-induced cellular toxicity. In addition, Rab8 – the *Drosophila* ortholog of Rab8a – ameliorated  $\alpha$ S-oligomer specific locomotor impairment and neuron loss in fruit flies. In support of the pathogenic relevance of the  $\alpha$ S-Rab8a interaction, phosphorylation of  $\alpha$ S at S129 enhanced binding to Rab8a, increased formation of insoluble  $\alpha$ S aggregates and reduced cellular toxicity. Our study provides novel mechanistic insights into the interplay of the GTPase Rab8a and  $\alpha$ S cytotoxicity, and underscores the therapeutic potential of targeting this interaction.

## INTRODUCTION

α-Synuclein (αS) is a widely abundant protein in the central nervous system<sup>1,2</sup>. Multiplications of the SNCA gene, which encodes αS<sup>3</sup>, as well as point mutations in □ Disease that is autosomal do affects several brain areas during its progression<sup>5</sup>. In addition, insoluble aggregated αS is the major component of Lewy bodies<sup>6</sup>. During the last decade a growing body of evidence suggested that the toxic species of αS are pre-fibrillar misfolded forms rather than insoluble neuronal deposits as found in Lewy bodies<sup>7-11</sup>. One prevalent hypothesis attributes the toxicity of αS oligomers to their high membrane affinity, which might cause membrane distortion and membrane leakage<sup>10,12-14</sup>.

Monomeric αS is intrinsically disordered and comprises 140 amino acids that distribute in three distinct domains: a basic N-terminal region (residues 1-60), a hydrophobic central domain (residues 61-95) and the acidic C-terminus (residues 96-140)<sup>15</sup>. Intra- and intermolecular contacts can be detected in monomeric, unfolded αS and are implicated in modulating the aggregation propensity<sup>16-19</sup>. The negatively charged C-terminus remains disordered in several conformational states such as monomeric, fibrillar and membrane-bound αS<sup>20-24</sup>. In Lewy bodies, 90% of αS is estimated to be phosphorylated at S129 in the C-terminus<sup>25</sup>. However, the functional role of this phosphorylation is largely unknown<sup>26,27</sup>. The C-terminus is also important in regulating αS aggregation through different modifications, such as ligand-binding<sup>28,29</sup> and truncation<sup>30-32</sup>.

The precise function of αS remains equivocal<sup>33</sup>, but several lines of evidence suggest that αS is involved in vesicle trafficking<sup>13,34,35</sup>. αS was reported to assist synaptic vesicle recycling, neurotransmitter release<sup>36,37</sup> and the function of SNAREs<sup>38</sup>. Moreover, αS was suggested to have a role in the maintenance of synaptic vesicle pools<sup>39,40</sup>, activity-dependent dopamine release<sup>41</sup> and to act as a negative regulator of vesicle priming<sup>42</sup>. In line with a role in vesicle trafficking, altering the expression levels and biophysical properties of αS and its familial mutants leads to deficits in vesicle trafficking at multiple stages in PD model systems<sup>13</sup>.

Rab GTPases are small guanine nucleotide binding proteins that play a key role in coordinating vesicle trafficking<sup>43</sup>, and have been associated with αS-related neuronal dysfunction<sup>44-51</sup>. In cellular and animal models of PD, αS overexpression disrupts vesicle trafficking between the endoplasmic reticulum (ER) and Golgi and overexpression of Rab1 attenuated αS toxicity<sup>52</sup>. Furthermore, Rab homeostasis is generally disturbed by αS in yeast with overexpression of Rab8a, Rab1 and Rab3a being partially protective against αS-induced toxicity<sup>53</sup>. In particular, Rab8a – the Rab GTPase that is responsible for modulating post-Golgi vesicle trafficking – increased the number of □ Overexpressing *C.elegans* with wild-type neurons from 15% to 40%, the strongest rescue effect found so far in this PD model<sup>53</sup>.

## Experimental section

### *Sample expression and purification*

Unlabeled and  $^{15}\text{N}$ -labeled  $\alpha\text{S}$  was expressed and purified as described previously <sup>54</sup>. Samples used for NMR spectroscopy contained  $^{15}\text{N}$ -labeled  $\alpha\text{S}$  in 50mM HEPES buffer, 100mM NaCl at pH 7.4.  $\alpha\text{S}$  was phosphorylated at S129 by polo-like kinase 3 (PLK3) at 30 °C and reached full phosphorylation after two hours in agreement with previous studies <sup>55</sup>. Phosphorylated  $\alpha\text{S}$  (pS129- $\alpha\text{S}$ ) was purified by semipreparative reverse-phase HPLC. Sample purity was tested by mass spectrometry. The C-terminal peptide of  $\alpha\text{S}$  (113-140) with phosphorylation at S<sup>129</sup> was synthesized using standard solid-phase fluorenylmethoxycarbonyl chemistry. The peptide was purified by semipreparative reverse-phase HPLC, and the purity (>95%) was analyzed by MS.

The human Rab8a gene was synthesized as codon-optimized DNA for expression in *Escherichia coli* (MR GENE, Regensburg, Germany). Full length Rab8a was subcloned into a modified pET19 vector that contained an N-terminal hexa-histidine tag and a Tobacco Etch Virus (TEV) protease cleavage sequence. To label Rab8 with  $^{15}\text{N}$  and  $^{13}\text{C}$  isotopes, the Rab8a construct was co-expressed with a plasmid encoding for GroES/ES chaperones (described previously in Bleimling et al., 2008) in *E. coli* BL21(DE3) in minimal medium containing 1 g/L  $^{15}\text{NH}_4\text{Cl}$  and 1 g/L  $^{13}\text{C}$ -D-Glucose. The purification of Rab8a was performed as described previously <sup>56</sup>. The preparation of GppNHp loaded Rab8a was performed as described <sup>57</sup>.

### *Co-Immunoprecipitation of Rab8 and $\alpha\text{S}$*

Immunoprecipitation (IP) experiments were performed using lysates from rat hippocampus and mouse cortical synaptosomes <sup>58</sup>. Dissected brain samples were homogenized in IP buffer (50 mM Tris-HCl pH7,5; 0,5 mM EDTA; 150 mM NaCl; 0,05 % NP40) freshly supplemented with protease inhibitors (Roche Diagnostics, Mannheim, Germany). Lysates were pre-cleared by incubation with 20  $\mu\text{l}$  of protein G beads (Invitrogen, Barcelona, Spain) for 30 min at 4 °C. The supernatants were incubated overnight at 4 °C with rotation either with anti-synuclein (10  $\mu\text{g}/\text{ml}$ ; Santa Cruz Biotechnology, rabbit) or with anti-Rab8 antibody (10  $\mu\text{g}/\text{ml}$ ; BD Bioscience, mouse). The immune complexes were then adsorbed for 3 hours to protein G agarose beads at 4 °C. Next, beads were washed according to the manufacturer's recommendation, resuspended in Laemmli buffer and heated at 100 °C for 5 min. The resulted supernatants were resolved on a 12 % SDS-PAGE gel. After transferring proteins in nitrocellulose membranes, membranes were blocked and incubated overnight

with the respective primary antibody, anti-synuclein (1:1000; Santa Cruz Biotechnology, rabbit) or anti-Rab8 (1:1000; BD Bioscience, mouse). Membranes were then incubated with secondary antibody (HRP-conjugated anti-mouse; GE Healthcare, Bucks, UK, 1:10,000). The immunoreactivity was visualized by chemiluminescence using an ECL detection system (Millipore, Billerica, MA, USA).

### ***NMR experiments***

NMR spectra were acquired at 15°C on a Bruker Avance 600 NMR spectrometer using a triple-resonance cryoprobe equipped with z-axis self-shielded gradient coils. Low temperature (15°C) reduces aggregation of  $\alpha$ S and the impact of amide proton exchange. Rab8a binding was followed using two-dimensional  $^1\text{H}$ - $^{15}\text{N}$  HSQC experiments with 1024 and 512 complex points in the direct and indirect dimension, respectively, 32 scans per increment and a recovery delay of 1.2 s. Spectral widths were 8389 Hz and 1809 Hz. Average  $^1\text{H}/^{15}\text{N}$  chemical shift perturbations were calculated according to  $[(\Delta\sigma^1\text{H})^2 + (\Delta\sigma^{15}\text{N})^2 / 25]$ , where  $\Delta\sigma^1\text{H}$  and  $\Delta\sigma^{15}\text{N}$  are the observed changes in  $^1\text{H}$  and  $^{15}\text{N}$  chemical shifts.

For backbone resonance assignment of Rab8a, relaxation-optimized versions of 3D NMR experiments HNCA, HNCACB, CBCA(CO)NH were recorded on  $^{13}\text{C}$ ,  $^{15}\text{N}$ -labelled Rab8a at a Bruker Avance 800 NMR spectrometer. In addition, 3D HNCOC and HN(CA)CO experiments were recorded for the C-terminal truncated Rab8a variant, Rab8a- $\delta$ C. Based on the 3D spectra, assignment of  $\text{C}\alpha$ ,  $\text{C}\beta$ , N, HN chemical shifts was obtained by an iterative procedure of automatic assignment using the program MARS<sup>59,60</sup> and manual verification and extension of the assignment.

### ***$\alpha$ S fibrillization***

Aggregation of  $\alpha$ S was carried out in 50 mM HEPES, 100 mM NaCl, 0,01 %  $\text{NaN}_3$ , pH 7.4. Larger species other than monomeric proteins were removed prior to aggregation using a 0.22  $\mu\text{m}$  membrane filter (Millipore, Billerica, MA, USA) followed by centrifugation at 60000 rpm for 2 h at 4°C using a Beckman 17 ultracentrifuge equipped with TLA.100 rotor (Beckman Coulter, South Kraemer Boulevard Brea, CA, USA). A volume of 300  $\mu\text{l}$  of freshly prepared protein solution was incubated at 21°C in glass vials under constant mixing with micro-stirring bars. Rab proteins were added prior to the start of aggregation at the specified molar ratio. At different time points, 5  $\mu\text{l}$  aliquots were taken from the aggregating sample and added into 2 ml of 5  $\mu\text{M}$  ThT in 50 mM Na-glycine, pH 8.2. ThT fluorescence was measured on a Varian Cary Eclipse spectrofluorimeter using 3.5 ml quartz cuvettes (Hellma, Jena, Germany) with an

excitation wavelength of 446 nm and emission at 480 nm. Error bars were calculated from three independent aggregation assays.

### ***Transmission Electron Microscopy***

For negative staining, a protein-containing solution was applied to glow-discharged carbon coated grids and stained with 1% uranyl acetate. Images were taken with a Philips CM120 electron microscope (Philips Inc.) at a defocus of 2.3  $\mu\text{m}$  using a TemCam 224A slow scan CCD camera (TVIPS, Gauting, Germany).

### ***Cell culture and transfection***

Neuroglioma H4 cells were maintained at 37°C and 5% CO<sub>2</sub> in Optimem medium (Gibco) supplemented with 10% Fetal Calf Serum and 1% penicillin-streptomycin. Cells were seeded, one day prior to transfection in either 24-well plate, for western blot and cytotoxicity assay, or  $\mu$ -Dish 35 mm Ibidi dishes for immunocytochemistry. Triple transient transfections of  $\alpha\text{S}$ , synphilin-1 and either Rab8a or GFP were performed with Fugene 6 (Promega) according to manufacturer's instructions.

### ***Site-directed mutagenesis***

SynT S129D and SynT S129A were generated by site directed mutagenesis (QuickChange II Site-Directed Mutagenesis Kit, Agilent Technologies) using SynT as template. The selected primers for S129D were: “GGC TTA TGA AAT GCC TGA TGA GGA AGG GTA TCA AG” and “CTT GAT ACC CTT CCT CAT CAG GCA TTT CAT AAG CC” while for S129A the primers were “CTT ATG AAA TGC CTG CTG AGG AAG GGT ATC” and “CTT ATG AAA TGC CTG CTG AGG AAG GGT ATC” forward and reverse respectively.

### ***Immunocytochemistry***

For immunofluorescence microscopy cells were fixed with 4% paraformaldehyde (PFA) 48 hours after transfection, sequentially treated with 0.5% trinton X-100 and 1,5% normal goat serum in PBS. Cells were incubated with anti- $\alpha\text{S}$

antibody (BD 610787, 1:1000) at 4°C overnight, followed by incubation with Alexa Fluor donkey anti-mouse 555 (Invitrogen A31570, 1:1000) secondary antibody. Before visualization, cells were stained with Hoechst (Molecular Probes 33258). Images were captured, in a blind process, using a Leica DMI 6000B microscope (Leica, Wetzlar, Germany) and analyzed with Image J software (NHI, USA). For counting the number of aggregates per cell, three different categories were chosen: cells with no aggregates, cells with less than 10 aggregates and cells with 10 or more aggregates.

NIAD-4 staining (Glixs labs, USA), to identify the presence of amyloid-like structures, was performed by incubating cells with the dye at a final concentration of 10µM for 30min at room temperature followed by immunocytochemistry as previously described.

### ***Cytotoxicity assay***

Cytotoxicity was measured via release of LDH into the culture medium with the Cytotoxicity Detection Kit (LDH) (Roche, Mannheim, Germany). Basic LDH release was measured in non-transfected cells, the maximal LDH release was measured by cell lysis in 2% Triton X-100. Absorbance was measured with the Infinite M2000 PRO (Tecan, Mainz, Germany) plate reader at 490 nm. Experimental values were calculated in percentages of the maximal LDH release and normalized to empty vector (pSI).

### ***Immunoblotting analysis***

Cell lysates were electrophoresed through 15% polyacrylamide gels, then transferred to nitrocellulose membranes (GE Healthcare) and blocked with 5% skim milk. Membranes were then incubated with primary antibodies (anti-αS, BD, 1:4000; anti-Rab8a, BD, 1:4000 or anti-βactin, Sigma-Aldrich, A-5441, 1:10000) overnight at 4° C. HRP-conjugated secondary antibodies (GE Healthcare, NXA 931, 1:10000) were applied for 1 hour at room temperature and visualized on Alpha Imager (Alpha Innotech).

### ***Fly stocks***

Flies were maintained on standard maize food at 25°C in LD 12:12. The *w; +; ple-GALA* (8848), *w; UASRab8-YFP; +* (9782), *w; +; UAS $\alpha$ S<sub>wt</sub>* and *w; UASeGFP; +* (5431) lines were obtained from the Bloomington Stock Center (Indiana). The *c164-GALA* driver was kindly donated by Juan Botas (Baylor College of Medicine). The *UASlacZ*, *UAS $\alpha$ S<sub>wt</sub>* and *UAS $\alpha$ S<sub>TPs</sub>* were a gift from Alf Herzig (Max-Planck-Institut für Biophysikalische Chemie).

### ***Larval crawling assay***

Briefly, crosses were set up in standard maize fly food mixed with 0.05% Bromophenol Blue (FisherBiotech) as described previously<sup>61</sup>. Young deep blue colored third instar wandering larvae were used for the crawling assay. Each larva was washed in distilled water and placed in the middle of a 145 mm petri dish coated with 0.8% agarose. The distance covered by the larva in 2 minutes was manually tracked on a transparent sheet placed on the top of the petri dish lid. The tracks were scanned and the distance calculated using Image J software (<http://rsbweb.nih.gov/ij/>).

### ***Negative geotaxis assay***

Negative geotaxis was determined in flies as previously described<sup>62</sup>. Ten days old flies were placed in a cylinder consisting of two empty fly vials taped together at their open ends. An 8 cm line was drawn from one end defining the threshold that flies must reach in order to be scored. Prior to initiating trials, flies were acclimatised to the apparatus for 1 minute, and then the tube was tapped gently in order to gather the flies at the bottom of the tube. The flies were permitted to fly or scale the sides of the tube for 10 seconds and the number of flies passing the threshold recorded. The experiment was repeated 10 times, with a one minute rest in between trials.

### **Detection of dopaminergic neurons in *Drosophila* by immunocytochemistry**

Adult flies aged to 30 days post-eclosion were collected and fixed overnight at 4°C in 4% formaldehyde-PBS containing 0.5% of Triton X-100. Brains were dissected in ice-cold PBS and further permeabilised with 3 X 20 min washes with PBST (with 1% Triton X-100). Brains were then blocked with 10% goat serum in PBST for at least 1 h and incubated overnight at 4°C with mouse anti-TH antibody (1:100, Immunostar). Before and after the secondary antibody incubation

(anti-mouse Cy5, 1:500, Abcam), brains were washed for 20 min with PBST. A solution of 3% N-propylgallate and 80% glycerol in PBS was used for mounting the samples which were then visualized and analysed on an Olympus FV1000 confocal microscope and processed with Olympus software, respectively.

## RESULTS

### **$\alpha$ S interacts with Rab8a in rodent brain**

To determine whether  $\alpha$ S and Rab8a interact at endogenous levels in the brain, we performed co-immunoprecipitation assays. Immunoprecipitation (IP) of  $\alpha$ S pulled down Rab8a both in rat hippocampus and mouse cortical synaptosomes (Figure 1A) while no signal was observed in the control IP with rabbit serum, demonstrating the specificity of the IP (Supplementary Figure 1). Furthermore, in mouse cortical synaptosome preparations, immunoprecipitation of Rab8a successfully pulled down  $\alpha$ S (Figure 1B). These results concluded that  $\alpha$ S and Rab8a interact under physiological conditions and the interaction occurs also in the synaptic compartment.

### **The C-terminus of $\alpha$ S binds to the switch 1 and 2 regions of Rab8a**

To obtain molecular insight into the binding of Rab8a to  $\alpha$ S, we employed nuclear magnetic resonance (NMR) spectroscopy. NMR resonances are highly sensitive probes of protein-protein and protein-ligand interactions and therefore allow a detailed description of interaction interfaces and binding affinities<sup>63</sup>.  $\alpha$ S and Rab8a were produced recombinantly and changes in chemical shifts and signal intensities were followed in two-dimensional <sup>1</sup>H-<sup>15</sup>N correlation spectra (heteronuclear single quantum coherence, HSQC) of  $\alpha$ S. Significant changes in NMR signals were observed for residues G111 to A140 of  $\alpha$ S (Figure 2A). In both the GDP- and GppNHp- (a hydrolysis-resistant structural analogue of GTP) bound states, Rab8a selectively interacted with the acidic C-terminus of  $\alpha$ S (Figures 2A, 2B). Dissociation constants,  $K_d$ , for the interaction were determined from the concentration-dependent chemical shift changes of the strongly affected and well-resolved  $\alpha$ S resonances of A124, Y125, E126, M127, D134 and E137:  $K_d$  values for Rab8a(GDP) and Rab8a(GppNHp) binding to  $\alpha$ S were  $0.19 \pm 0.01$  mM and  $0.45 \pm 0.05$  mM, respectively. Thus, the GDP-bound state of Rab8a binds slightly stronger to  $\alpha$ S than the GppNHp-bound form.

To identify the binding site of  $\alpha$ S on Rab8a, we determined the sequence-specific backbone resonance assignment of Rab8a(GDP). In the <sup>15</sup>N-<sup>1</sup>H HSQC of Rab8a, 175 backbone signals for 207 non-proline residues were observed (Figure

3A). The remaining residues are probably not detectable due to conformational flexibility, in line with the known dynamic nature of the switch 1 and switch 2 regions of Rab proteins in the GDP-bound state<sup>64</sup>. 161 out of these signals could be assigned unambiguously. Based on the resonance assignment, the titration of Rab8a(GDP) with  $\alpha$ S revealed that residues in the G2 loop, as well as the observable residues of the  $\alpha$ S binding site, showed changes in NMR signal positions as a result of  $\alpha$ S binding (Figure 3B). In addition, these residues showed increased signal intensities, indicating changes in backbone dynamics in the switch 1/2 region upon  $\alpha$ S binding (Figure 3C, 3D). Rab8a has previously been suggested to be highly dynamic and to experience large conformational changes between different nucleotide states<sup>64</sup>. Inspection of the 3D structure of Rab8a showed that the G2 loop is part of a positively charged surface patch (Figure 3E). Besides changes in the switch 1/2 region, NMR resonances of residues A173-G181 and I193-T194 at the positively charged C-terminus of Rab8a were perturbed upon addition of  $\alpha$ S (Figures 3B,C). Thus, the C-terminus of Rab8a might provide a second independent binding site, as very similar chemical shift changes were observed in the switch 1/2 region when using a Rab8a variant, Rab8a- $\delta$ C, truncated at position 178 (Supplementary Figure S2).

### Phosphorylation at S129 tightens the $\alpha$ S-Rab8a interaction

Phosphorylation at S129 (pS129) (Figure 4A) is the most abundant post-translational modification of  $\alpha$ S in PD<sup>25,65</sup>. Titration of pS129- $\alpha$ S to Rab8a(GDP) revealed that, at the same molar ratio, Rab8a caused stronger NMR signal attenuation in pS129- $\alpha$ S than in wild-type  $\alpha$ S (Figures 4B, 4C). In particular, the resonance of phosphorylated S129 completely disappeared (Figure 4B), indicating that it is strongly involved in the interaction. In line with a phosphorylation-dependent regulation of the  $\alpha$ S-Rab8a interaction, the S129D variant of  $\alpha$ S, which is widely used to mimic phosphorylation *in vivo*<sup>27</sup>, results in signal attenuation stronger than the wild-type protein (Figure 4C). Taken together, the NMR data demonstrate that phosphorylation of  $\alpha$ S at S129 promotes binding of  $\alpha$ S to Rab8a.

### Rab8a enhances $\alpha$ S fibrillization

Aggregation of  $\alpha$ S is a key event in the pathogenesis of PD. Following identification of the Rab8a/ $\alpha$ S interaction, we investigated the role of Rab8a in modulating  $\alpha$ S aggregation *in vitro* and in cells. First,  $\alpha$ S was incubated *in vitro* with full-length Rab8a(GDP) under aggregation-promoting conditions and fibrillization kinetics were monitored using the amyloid-specific dye Thioflavin T (ThT). Rab8a(GDP) enhanced fibrillization of  $\alpha$ S at different Rab8a(GDP): $\alpha$ S molar

ratios (Figure 5A). Already at a Rab8a(GDP): $\alpha$ S molar ratio of 0.5:1 the lag phase of fibrillization was reduced from 24 hours to 15 hours. Even more dramatic, however, was the increase in the rate of  $\alpha$ S fibrillization at (Figure 5A). Incubation of Rab8a alone did not result in enhanced ThT activity (Supplementary Figure S3), excluding a significant contribution of Rab8a aggregation to the ThT signal.

Electron microscopy (EM) was used to morphologically assess the fibrillar species formed by  $\alpha$ S in the absence and presence of Rab8(GDP) (Figures 5B-D). Compared to fibrils of  $\alpha$ S alone,  $\alpha$ S fibrils in the presence of Rab8a were shorter and had a tendency to stick together. In addition, with increasing amounts of Rab8a roundish clumps were visible on the fibrillar surface, suggesting that Rab8a might bind to  $\alpha$ S fibrils. An interaction of Rab8a with the C-terminus of fibrillar  $\alpha$ S appears possible, as a variety of investigations have shown that the C-terminus of  $\alpha$ S remains disordered and accessible in  $\alpha$ S fibrils <sup>21,22</sup>.

### **Rab8a enhances cellular $\alpha$ S aggregation and reduces $\alpha$ S-induced toxicity**

To obtain further insight into the effect of Rab8a on  $\alpha$ S aggregation and  $\alpha$ S-induced toxicity, we used a previously described cell model (Figure 6A) <sup>66</sup> that accumulates amyloid-like  $\alpha$ S structures, as demonstrated by staining with NIAD-4, an amyloid-binding dye (Figure 6D) <sup>67</sup>. We observed that endogenous and overexpressed Rab8a co-localized with  $\alpha$ S-positive inclusions (Supplementary Figure S4). In addition, overexpression of Rab8a resulted in a 30% increase in the number of cells with inclusions (Figure 6B), in line with Rab8a-promoted fibrillization of  $\alpha$ S *in vitro* (Figure 5). Strikingly, the S129D mutant of  $\alpha$ S, which carries a negative charge in position 129 to mimic phosphorylation and which binds more strongly to Rab8a (Figure 4), further increased the number of inclusions per cell in the presence of Rab8a (Figure 6C). On the other hand, the S129A mutant that blocks phosphorylation, showed an increase in the percentage of cells with no aggregates (Figure 6C). Taken together the data suggest both a role for Rab8a and  $\alpha$ S phosphorylation in the process of  $\alpha$ S aggregation in a cellular context.

Next, we investigated whether Rab8a also influenced toxicity in the same cell model that was used for analysis of  $\alpha$ S aggregation. Toxicity was determined 48 hours after transfection by release of lactate dehydrogenase (LDH) into the medium. Our experiments showed that overexpression of Rab8a increased toxicity only moderately relative to control transfections, while  $\alpha$ S overexpression resulted in a more than two-fold increase in toxicity (Figure 7A). However, when Rab8a and  $\alpha$ S were coexpressed, cellular toxicity decreased significantly when compared to  $\alpha$ S alone (Figure 7A). Notably, overall protein levels were not affected by coexpression of the proteins, ruling out the possibility that the

observed protection was due to a reduction in the levels of  $\alpha$ S (Figure 7B). In case of the S129D mutant of  $\alpha$ S, cellular toxicity was further reduced when coexpressed with Rab8a (Figure 7A). We also observed a reduction in toxicity with the S129A mutant, but this effect might also be related with the effect of the mutant on aggregation, since it leads to a reduction in the percentage of cells displaying inclusions (Figure 7A and Figure 6).

### **Rab8 ameliorates $\alpha$ S-dependent behavioural defects in fruit flies**

We next investigated overexpression of Rab8 - the *Drosophila melanogaster* ortholog of Rab8a – in two robust fruit fly models of  $\alpha$ S toxicity. The first is a widely used model in which the transgene encoding  $\alpha$ S was inserted randomly into the genome using P-element based transgenesis<sup>68</sup>, and the second is a more recent model we generated in which individual transgenes encoding wild-type or mutant versions of  $\alpha$ S were targeted into a specific genomic location using the  $\phi$ C31-based site specific recombination system, reducing positional effects and eliminating insertional mutagenesis concerns<sup>10</sup>.  $\alpha$ S expression has been extensively studied in flies as a model of PD, and yields several disease-relevant phenotypes, including formation of Lewy bodies, dopaminergic neuron loss, locomotor impairments, and abnormal circadian rhythmicity<sup>10,68-70</sup>. Here, we took advantage of the GAL4/UAS bitransgenic system to drive expression of  $\alpha$ S in moto- and dopaminergic neurons using *c164* and *ple* drivers, respectively, and to study locomotor behaviour of third instar larvae. Expression of  $\alpha$ S in these tissues caused a significant reduction in the distance crawled by the larvae compared to controls (Figure 8). Coexpression of Rab8 with  $\alpha$ S in either motoneurons or dopaminergic neurons dramatically rescued this phenotype ( $p < 0.01$  and  $p < 0.001$ , respectively, Figure 8A and 8B). In order to exclude that the observed rescue was due to titration effects caused by the presence of multiple UAS transgenes, we also analysed the crawling behaviour in larvae co-expressing both eGFP and  $\alpha$ S, and found no difference with the larvae expressing  $\alpha$ S alone, further supporting a protective role of Rab8.

We then validated Rab8 protection using our recently-developed  $\phi$ C31  $\alpha$ S lines. The lines tested carry a transgene expressing either wild-type  $\alpha$ S or a pre-fibrillar mutant in which three alanines are substituted with proline residues (TP)<sup>70</sup>. A significant decrease in larval crawling was observed when either WT or TP  $\alpha$ S was expressed in the motoneurons ( $p < 0.001$ , Figure 8C) or dopaminergic neurons ( $p < 0.001$ , Figure 8D). Overexpression of Rab8 was protective in flies expressing both  $\alpha$ S forms in either neuronal population tested (Figure 8C, D).

To further explore locomotor activity we performed climbing assays in adult flies, which measure negative geotaxis<sup>62</sup>. We found that ten day old flies pan-neuronally expressing  $\alpha$ S via the *elavGAL4* driver exhibit a significant ~55% reduction in climbing compared to controls ( $p < 0.001$ , Figure 9). Strikingly, coexpression of Rab8 with  $\alpha$ S strongly rescued this locomotor impairment ( $p < 0.001$ ), supporting our observations in larvae, and indicating that Rab8 is able to reverse  $\alpha$ S-dependent behavioural phenotypes in an animal model (Figure 9).

Finally we investigated whether Rab8A could reverse the loss of dopaminergic neurons caused by the expression of  $\alpha$ S. The adult *Drosophila* brain possesses several dopaminergic neuron clusters which are classified depending on their brain region localization<sup>71</sup>. We focused our analyses on three clusters of neurons located on the posterior inferiormedial protocerebrum, the PPL<sub>1</sub>, PPM<sub>2</sub> and PPM<sub>3</sub> neurons. We found that the expression of  $\alpha$ S with either the *elav* or *ple* driver caused a significant reduction of neurons in the PPL<sub>1</sub> cluster (Figure 10,  $p < 0.01$ ). We also observed a significant reduction of in the PPM<sub>3</sub> neurons ( $p < 0.05$ ), whereas the PPM<sub>2</sub> group appeared to be only marginally affected by the expression of  $\alpha$ S (right and middle panels in Figure 10, respectively). Strikingly, the co-expression of Rab8 with  $\alpha$ S fully rescued the loss of dopaminergic PPL<sub>1</sub> neurons with either driver ( $P < 0.05$ ). In addition, the loss of PPM<sub>3</sub> neurons was partially rescued by Rab8 co-expression with the *elav* driver ( $P < 0.01$ ).

## DISCUSSION

Increasing evidence suggests that defects in vesicular trafficking are important for the pathogenic events leading to PD<sup>13,34,35</sup>. Several Rab GTPases were suggested to interact aberrantly with  $\alpha$ S in Dementia with Lewy Bodies<sup>46,72,73</sup>. In addition, Rab proteins colocalize with glial inclusions containing  $\alpha$ S in multiple system atrophy<sup>74,75</sup>, Rab GTPases were found in vesicle clusters induced by  $\alpha$ S overexpression in yeast<sup>53</sup>, and overexpression of the Rab GTPases Rab1, Rab3a and Rab8a decreased  $\alpha$ S-induced neurotoxicity<sup>52,53</sup>. The Rab GTPases Rab8a, which showed the strongest rescue of  $\alpha$ S-toxicity in the nematode PD model<sup>53</sup>, is associated with recycling endosomes and basolateral trafficking events from the trans Golgi network to the plasma membrane<sup>76</sup>. Also, Golgi fragmentation was recently shown to be Rab and SNARE dependent in cellular models of PD, further linking Rab8 with  $\alpha$ S<sup>77</sup>. Although the genetic variant A30P  $\alpha$ S has been observed to co-precipitate with Rab8 in transgenic mice<sup>45</sup>, no direct interaction between Rab8a, or any other Rab GTPase, with  $\alpha$ S has been reported thus far. Here we demonstrated that  $\alpha$ S is associated with Rab8a in the rat hippocampus as well

as mouse cortical synaptosomes (Figure 1). NMR spectroscopy revealed the molecular details of the interaction and linked key sites of the two proteins - that is the C-terminus of  $\alpha$ S and the switch 1/2 region of Rab8a (Figures 2, 3). The pathological relevance of the interaction is supported by the observation that phosphorylation of S129 in  $\alpha$ S enhances the binding (Figure 4) and modulates the influence of Rab8a on  $\alpha$ S aggregation and cellular toxicity (Figures 6, 7). It remains to be seen if other Rab proteins can directly bind to  $\alpha$ S *in vitro* and *in vivo* and whether their effect on  $\alpha$ S-related neurotoxicity is mediated by a direct interaction.

The switch between the GDP- and GTP-bound state of Rab proteins is a fundamental process influencing a wide range of protein functions<sup>43</sup>. Our NMR data revealed that Rab8a binds to  $\alpha$ S in both states, but with a slightly stronger affinity towards Rab8a (GDP) (Figure 2). The interaction occurs between the C-terminus of  $\alpha$ S and the switch 1/2 region of Rab8a (Figure 3). The importance of the interaction with the switch 1/2 region was supported by interaction studies employing a Rab8a variant lacking the C-terminal tail (Supplementary Figure S2). The switch 1/2 region of Rab8a is predominantly positive and provides a favorable binding surface for the negatively charged C-terminal domain of  $\alpha$ S (Figure 3E). Notably, the major structural change between the two nucleotide-bound states of Rab proteins occurs in this region with the GTP-bound state being more rigid<sup>64,78</sup>. Thus, different conformations of the switch region and in particular the G2 loop of Rab8a might contribute to the higher affinity of  $\alpha$ S towards Rab8a(GDP) (Figure 2). The difference in affinity suggests that the GTP-bound state of Rab8a is less affected by overexpression of  $\alpha$ S. On the other hand, GTP-bound Rab proteins interact with many effector proteins, while inactive Rab proteins are complexed with guanine nucleotide dissociation inhibitor proteins<sup>64</sup>. Thus,  $\alpha$ S needs to compete with a variety of Rab8a binding partners. In addition, GTP-bound Rab proteins are anchored to membranes via a C-terminal lipid anchor<sup>79</sup>, and only leave the membrane upon hydrolysis to GDP. Thus, new interactions with the flex of membrane-bound  $\alpha$ S might arise in the GTP-bound membrane-anchored state of Rab8a. In line with its cytosolic state, however, we found a preferential interaction with GDP-bound Rab8a in our *in vitro* measurements, which employed soluble Rab8a and  $\alpha$ S. In addition, it is important to keep in mind that  $\alpha$ S is highly abundant in neuronal systems<sup>1,2</sup> and a large excess of  $\alpha$ S could favor binding to Rab8a. Indeed, triplication of the  $\alpha$ S locus was shown to cause PD and  $\alpha$ S progressively accumulates in cytosolic vesicles and the ER during disease<sup>52,80</sup>. Moreover, the C-terminal tail of Rab8a is less affected by nucleotide and membrane binding and can therefore - independent of other Rab8a interactions - contribute to the interaction with the C-terminal domain of  $\alpha$ S, which remains accessible in both the soluble and membrane-bound state and even in  $\alpha$ S fibrils<sup>20-22,24</sup>.

Aggregation of  $\alpha$ S into insoluble deposits is a hallmark of PD and is observed in cellular and animal models based on  $\alpha$ S overexpression<sup>81</sup>. Understanding the underlying toxicity of different  $\alpha$ S species in the aggregation pathway has been a major goal in the field. Although current theories suggest oligomeric species might constitute the most toxic species<sup>10,11,18</sup>, consensus is still lacking<sup>82,83</sup>. An undisputable fact, obtained from the clinical research, is that intracellular aggregates are found in the surviving neurons of PD patients indicating that their presence can, perhaps, have a beneficial effect in cell survival<sup>84</sup>. Our experiments show that overexpression of Rab8a in a cellular model increased the number of cells with  $\alpha$ S inclusions (Figure 6), in line with enhanced *in vitro* aggregation of  $\alpha$ S into amyloid fibrils in the presence of Rab8a (Figure 5). In addition, we found that mimicking  $\alpha$ S phosphorylation increased the number of inclusions per cell. NMR spectroscopy suggests that the enhanced aggregation is due to a direct binding of Rab8a to the C-terminus of  $\alpha$ S that has been implicated in interactions with a variety of protein partners<sup>31,85-90</sup>. Thus, our study provides a link between physiological  $\alpha$ S interactions and pathogenic aggregation. Moreover, Rab8a decreased  $\alpha$ S toxicity in our cell model while  $\alpha$ S levels remained unchanged (Figure 7), consistent with previous studies in which Rab8a was able to decrease  $\alpha$ S associated neuronal loss in a *Caenorhabditis elegans* model and in rat primary neuronal cultures<sup>53</sup>. Our finding that Rab8a dramatically improved  $\alpha$ S-dependent behavioral deficits in several *Drosophila* models (Figures 8 and 9) further supports these observations. Thus, a Rab8a-mediated increase in formation of insoluble  $\alpha$ S aggregates could constitute a mechanism underlying Rab8a-mediated cellular protection.

Phosphorylation of  $\alpha$ S at S129 is the most abundant post-translational modification in Lewy bodies<sup>25,65</sup>. S129 can be phosphorylated by a variety of kinases *in vitro* and *in vivo*<sup>91</sup>. In particular, polo-like kinases quantitatively and selectively phosphorylate  $\alpha$ S at S129 and levels of polo-like kinase 2 are increased in brains of patients with Lewy body disease<sup>55,92</sup>. However, the relevance of  $\alpha$ S phosphorylation at S129 for neurotoxicity and disease remains controversial<sup>93</sup>. While some reports report a beneficial effect<sup>94,95</sup>, others identified deleterious consequences<sup>96,97</sup>. A separate study found no effects of this post-translational modification<sup>98</sup>. Our study reveals that phosphorylation of  $\alpha$ S at S129 enhances the binding of  $\alpha$ S to Rab8a (Figure 4). This finding is in line with a previous observation that  $\alpha$ S phosphorylated at S129 is found specifically in pull downs with vesicular trafficking proteins<sup>99</sup>. Notably, the S129D variant of  $\alpha$ S also showed enhanced Rab8a binding (Figure 4), supporting its use for mimicking S129 phosphorylation *in vivo*. In addition, coexpression of S129D  $\alpha$ S with Rab8a enhanced aggregation of  $\alpha$ S in H4 cells to a larger degree than coexpression of *wt*  $\alpha$ S with Rab8a (Figure 6C) and reduced cellular toxicity (Figure 7A). In line with these findings, phosphorylation of  $\alpha$ S at S129 can – dependent on the genetic background – reduce  $\alpha$ S-induced defects in vesicle trafficking<sup>100</sup>. Thus, our study provides molecular insights into

the functional consequences of phosphorylation of  $\alpha$ S at S129 and supports the role of changes in protein-protein interactions for  $\alpha$ S pathogenicity<sup>99</sup>.

In summary, we have established a direct interaction between  $\alpha$ S and Rab8a and provided unique insights into the molecular mechanisms of  $\alpha$ S toxicity. Binding of  $\alpha$ S to the switch 1/2 region of Rab8a suggests that  $\alpha$ S can interfere with the physiological function of Rab GTPases, in particular when  $\alpha$ S levels are increased, and thus lead to deficits in vesicle trafficking. Phosphorylation at S129 enhances binding of  $\alpha$ S to Rab8a, increases aggregation of  $\alpha$ S into insoluble aggregates and reduces  $\alpha$ S-induced cellular toxicity. S129 phosphorylation can therefore critically influence the toxic interplay of Rab8a and  $\alpha$ S, further supporting the possibility of targeting phosphorylation as a therapeutic strategy in PD and other synucleinopathies.

**Abbreviations:**  $\alpha$ S, alpha-Synuclein; EM, electron microscopy; ER, endoplasmic reticulum; GDP, guanosine diphosphate; GTP, guanosine triphosphate; GppNHp, on-hydrolysable analogue of GTP; HSQC, heteronuclear single-quantum coherence; LDH, lactate dehydrogenase; NMR, nuclear magnetic resonance; PD, Parkinson Disease; Rab, Ras related in brain; Rab8a- $\square$ C, Rab8a (9-178); SNARE, soluble NSF attachment protein receptor; ThT, Thioflavin T.

## Acknowledgements

We thank Dr. Dietmar Riedel and Gudrun Heim for electron micrographs, Sebastian Wolff and Karin Giller for  $\alpha$ S sample preparation, Kerstin Overkamp for peptide synthesis, Nathalie Bleimling for Rab8a sample preparation and Pinar Karpinar for help in initial NMR measurements. The GFP-RAB8a plasmid was kindly provided by Dr. Mikael Simons. This work was supported by the BMBF (NGFN-Plus 01GS08190 to M.Z.). Tomas Lopes da Fonseca is supported by a fellowship from the Fundaao para a Ciencia e a Tecnologia, Portugal (SFRH/BD/74881/2010). Work in the laboratory of Flaviano Giorgini is supported by Parkinson's UK (G-1203). TFO is supported by the DFG Center for Nanoscale Microscopy and Molecular Physiology of the Brain. The authors declare that they have no conflict of interest.

## References

- 1 Jakes, R., Spillantini, M. G. & Goedert, M. Identification of two distinct synucleins from human brain. *FEBS Lett* **345**, 27-32, doi:0014-5793(94)00395-5 [pii] (1994).

- 2 Iwai, A. *et al.* The precursor protein of non-A beta component of Alzheimer's disease amyloid is a presynaptic protein of the central nervous system. *Neuron* **14**, 467-475, doi:0896-6273(95)90302-X [pii] (1995).
- 3 Chartier-Harlin, M. C. *et al.* Alpha-synuclein locus duplication as a cause of familial Parkinson's disease. *Lancet* **364**, 1167-1169, doi:10.1016/S0140-6736(04)17103-1 (2004).
- 4 Hardy, J., Lewis, P., Revesz, T., Lees, A. & Paisan-Ruiz, C. The genetics of Parkinson's syndromes: a critical review. *Curr Opin Genet Dev* **19**, 254-265, doi:S0959-437X(09)00055-0 [pii] 10.1016/j.gde.2009.03.008 (2009).
- 5 Braak, H. *et al.* Staging of brain pathology related to sporadic Parkinson's disease. *Neurobiol Aging* **24**, 197-211 (2003).
- 6 Spillantini, M. G. *et al.* Alpha-synuclein in Lewy bodies. *Nature* **388**, 839-840, doi:10.1038/42166 (1997).
- 7 Caughey, B. & Lansbury, P. T. Protofibrils, pores, fibrils, and neurodegeneration: separating the responsible protein aggregates from the innocent bystanders. *Annual review of neuroscience* **26**, 267-298 (2003).
- 8 Lashuel, H. A., Hartley, D., Petre, B. M., Walz, T. & Lansbury, P. T., Jr. Neurodegenerative disease: amyloid pores from pathogenic mutations. *Nature* **418**, 291 (2002).
- 9 Cookson, M. R. alpha-Synuclein and neuronal cell death. *Molecular neurodegeneration* **4**, 9 (2009).
- 10 Karpinar, D. P. *et al.* Pre-fibrillar alpha-synuclein variants with impaired beta-structure increase neurotoxicity in Parkinson's disease models. *The EMBO journal* **28**, 3256-3268, doi:10.1038/emboj.2009.257 (2009).
- 11 Winner, B. *et al.* In vivo demonstration that alpha-synuclein oligomers are toxic. *Proc Natl Acad Sci U S A* **108**, 4194-4199, doi:10.1073/pnas.1100976108 (2011).
- 12 Bodner, C. R., Dobson, C. M. & Bax, A. Multiple tight phospholipid-binding modes of alpha-synuclein revealed by solution NMR spectroscopy. *Journal of molecular biology* **390**, 775-790 (2009).
- 13 Auluck, P. K., Caraveo, G. & Lindquist, S. alpha-Synuclein: membrane interactions and toxicity in Parkinson's disease. *Annu Rev Cell Dev Biol* **26**, 211-233, doi:10.1146/annurev.cellbio.042308.113313 (2010).
- 14 Butterfield, S. M. & Lashuel, H. A. Amyloidogenic protein-membrane interactions: mechanistic insight from model systems. *Angewandte Chemie (International ed)* **49**, 5628-5654 (2010).
- 15 Polymeropoulos, M. H. *et al.* Mutation in the alpha-synuclein gene identified in families with Parkinson's disease. *Science* **276**, 2045-2047 (1997).
- 16 Bertocini, C. W. *et al.* Release of long-range tertiary interactions potentiates aggregation of natively unstructured alpha-synuclein. *Proc Natl Acad Sci U S A* **102**, 1430-1435 (2005).

- 17 Dedmon, M. M., Lindorff-Larsen, K., Christodoulou, J., Vendruscolo, M. & Dobson, C. M. Mapping long-range interactions in alpha-synuclein using spin-label NMR and ensemble molecular dynamics simulations. *Journal of the American Chemical Society* **127**, 476-477 (2005).
- 18 Outeiro, T. F. *et al.* Formation of toxic oligomeric alpha-synuclein species in living cells. *PLoS One* **3**, e1867, doi:10.1371/journal.pone.0001867 (2008).
- 19 Wu, K. P. & Baum, J. Detection of transient interchain interactions in the intrinsically disordered protein alpha-synuclein by NMR paramagnetic relaxation enhancement. *Journal of the American Chemical Society* **132**, 5546-5547, doi:10.1021/ja9105495 (2010).
- 20 Ulmer, T. S., Bax, A., Cole, N. B. & Nussbaum, R. L. Structure and dynamics of micelle-bound human alpha-synuclein. *J Biol Chem* **280**, 9595-9603, doi:M411805200 [pii] 10.1074/jbc.M411805200 (2005).
- 21 Del Mar, C., Greenbaum, E. A., Mayne, L., Englander, S. W. & Woods, V. L., Jr. Structure and properties of alpha-synuclein and other amyloids determined at the amino acid level. *Proc Natl Acad Sci U S A* **102**, 15477-15482, doi:0507405102 [pii] 10.1073/pnas.0507405102 (2005).
- 22 Vilar, M. *et al.* The fold of alpha-synuclein fibrils. *Proc Natl Acad Sci U S A* **105**, 8637-8642, doi:0712179105 [pii] 10.1073/pnas.0712179105 (2008).
- 23 Qin, Z., Hu, D., Han, S., Hong, D. P. & Fink, A. L. Role of different regions of alpha-synuclein in the assembly of fibrils. *Biochemistry* **46**, 13322-13330, doi:10.1021/bi7014053 (2007).
- 24 Eliezer, D., Kutluay, E., Bussell, R., Jr. & Browne, G. Conformational properties of alpha-synuclein in its free and lipid-associated states. *Journal of molecular biology* **307**, 1061-1073, doi:10.1006/jmbi.2001.4538 S0022-2836(01)94538-3 [pii] (2001).
- 25 Fujiwara, H. *et al.* alpha-Synuclein is phosphorylated in synucleinopathy lesions. *Nature cell biology* **4**, 160-164 (2002).
- 26 Oueslati, A., Fournier, M. & Lashuel, H. A. Role of post-translational modifications in modulating the structure, function and toxicity of alpha-synuclein: implications for Parkinson's disease pathogenesis and therapies. *Progress in brain research* **183**, 115-145 (2010).
- 27 Sato, H., Kato, T. & Arawaka, S. The role of Ser129 phosphorylation of alpha-synuclein in neurodegeneration of Parkinson's disease: a review of in vivo models. *Rev Neurosci*, 1-9, doi:10.1515/revneuro-2012-0071 /j/revneuro.ahead-of-print/revneuro-2012-0071/revneuro-2012-0071.xml [pii] (2013).

- 28 Fernandez, C. O. *et al.* NMR of alpha-synuclein-polyamine complexes elucidates the mechanism and kinetics of induced aggregation. *The EMBO journal* **23**, 2039-2046 (2004).
- 29 Goers, J., Uversky, V. N. & Fink, A. L. Polycation-induced oligomerization and accelerated fibrillation of human alpha-synuclein in vitro. *Protein Sci* **12**, 702-707, doi:10.1110/ps.0230903 (2003).
- 30 Hoyer, W., Cherny, D., Subramaniam, V. & Jovin, T. M. Impact of the acidic C-terminal region comprising amino acids 109-140 on alpha-synuclein aggregation in vitro. *Biochemistry* **43**, 16233-16242 (2004).
- 31 Kim, T. D., Paik, S. R. & Yang, C. H. Structural and functional implications of C-terminal regions of alpha-synuclein. *Biochemistry* **41**, 13782-13790 (2002).
- 32 Levitan, K. *et al.* Conserved C-terminal charge exerts a profound influence on the aggregation rate of alpha-synuclein. *Journal of molecular biology* **411**, 329-333 (2011).
- 33 Marques, O. & Outeiro, T. F. Alpha-synuclein: from secretion to dysfunction and death. *Cell Death Dis* **3**, e350, doi:cddis201294 [pii]  
10.1038/cddis.2012.94 (2012).
- 34 Lashuel, H. A., Overk, C. R., Oueslati, A. & Masliah, E. The many faces of alpha-synuclein: from structure and toxicity to therapeutic target. *Nat Rev Neurosci* **14**, 38-48, doi:nrn3406 [pii]  
10.1038/nrn3406 (2013).
- 35 Waxman, E. A. & Giasson, B. I. Molecular mechanisms of alpha-synuclein neurodegeneration. *Biochim Biophys Acta* **1792**, 616-624, doi:S0925-4439(08)00188-9 [pii]  
10.1016/j.bbadis.2008.09.013 (2009).
- 36 Ben Gedalya, T. *et al.* Alpha-synuclein and polyunsaturated fatty acids promote clathrin-mediated endocytosis and synaptic vesicle recycling. *Traffic (Copenhagen, Denmark)* **10**, 218-234 (2009).
- 37 Liu, S. *et al.* alpha-Synuclein produces a long-lasting increase in neurotransmitter release. *The EMBO journal* **23**, 4506-4516 (2004).
- 38 Chandra, S., Gallardo, G., Fernandez-Chacon, R., Schluter, O. M. & Sudhof, T. C. Alpha-synuclein cooperates with CSFalpha in preventing neurodegeneration. *Cell* **123**, 383-396 (2005).
- 39 Murphy, D. D., Rueter, S. M., Trojanowski, J. Q. & Lee, V. M. Synucleins are developmentally expressed, and alpha-synuclein regulates the size of the presynaptic vesicular pool in primary hippocampal neurons. *J Neurosci* **20**, 3214-3220 (2000).
- 40 Cabin, D. E. *et al.* Synaptic vesicle depletion correlates with attenuated synaptic responses to prolonged repetitive stimulation in mice lacking alpha-synuclein. *J Neurosci* **22**, 8797-8807 (2002).

- 41 Abeliovich, A. *et al.* Mice lacking alpha-synuclein display functional deficits in the nigrostriatal dopamine system. *Neuron* **25**, 239-252 (2000).
- 42 Larsen, K. E. *et al.* Alpha-synuclein overexpression in PC12 and chromaffin cells impairs catecholamine release by interfering with a late step in exocytosis. *J Neurosci* **26**, 11915-11922 (2006).
- 43 Stenmark, H. Rab GTPases as coordinators of vesicle traffic. *Nat Rev Mol Cell Biol* **10**, 513-525, doi:10.1038/nrm2728 nrm2728 [pii] (2009).
- 44 Dalfo, E., Barrachina, M., Rosa, J. L., Ambrosio, S. & Ferrer, I. Abnormal alpha-synuclein interactions with rab3a and rabphilin in diffuse Lewy body disease. *Neurobiology of disease* **16**, 92-97 (2004).
- 45 Dalfo, E. *et al.* Abnormal alpha-synuclein interactions with Rab proteins in alpha-synuclein A30P transgenic mice. *Journal of neuropathology and experimental neurology* **63**, 302-313 (2004).
- 46 Soper, J. H., Kehm, V., Burd, C. G., Bankaitis, V. A. & Lee, V. M. Aggregation of alpha-synuclein in *S. cerevisiae* is associated with defects in endosomal trafficking and phospholipid biosynthesis. *J Mol Neurosci* **43**, 391-405 (2011).
- 47 Liu, J. *et al.* Rab11a and HSP90 regulate recycling of extracellular alpha-synuclein. *J Neurosci* **29**, 1480-1485 (2009).
- 48 Chung, C. Y., Koprach, J. B., Hallett, P. J. & Isacson, O. Functional enhancement and protection of dopaminergic terminals by RAB3B overexpression. *Proc Natl Acad Sci U S A* **106**, 22474-22479 (2009).
- 49 Sancenon, V. *et al.* Suppression of alpha-synuclein toxicity and vesicle trafficking defects by phosphorylation at S129 in yeast depends on genetic context. *Hum Mol Genet* **21**, 2432-2449, doi:dds058 [pii] 10.1093/hmg/dds058.
- 50 Chen, R. H. *et al.* alpha-Synuclein membrane association is regulated by the Rab3a recycling machinery and presynaptic activity. *J Biol Chem*, doi:M112.439497 [pii] 10.1074/jbc.M112.439497 (2013).
- 51 Kuwahara, T. *et al.* A systematic RNAi screen reveals involvement of endocytic pathway in neuronal dysfunction in alpha-synuclein transgenic *C. elegans*. *Hum Mol Genet* **17**, 2997-3009, doi:ddn198 [pii] 10.1093/hmg/ddn198 (2008).
- 52 Cooper, A. A. *et al.* Alpha-synuclein blocks ER-Golgi traffic and Rab1 rescues neuron loss in Parkinson's models. *Science* **313**, 324-328, doi:1129462 [pii] 10.1126/science.1129462 (2006).

- 53 Gitler, A. D. *et al.* The Parkinson's disease protein alpha-synuclein disrupts cellular Rab homeostasis. *Proc Natl Acad Sci U S A* **105**, 145-150, doi:0710685105 [pii]  
10.1073/pnas.0710685105 (2008).
- 54 Hoyer, W. *et al.* Dependence of alpha-synuclein aggregate morphology on solution conditions. *Journal of molecular biology* **322**, 383-393 (2002).
- 55 Mbefo, M. K. *et al.* Phosphorylation of synucleins by members of the Polo-like kinase family. *J Biol Chem* **285**, 2807-2822 (2010).
- 56 Bleimling, N., Alexandrov, K., Goody, R. & Itzen, A. Chaperone-assisted production of active human Rab8A GTPase in *Escherichia coli*. *Protein Expr Purif* **65**, 190-195 (2009).
- 57 Hou, X. *et al.* A structural basis for Lowe syndrome caused by mutations in the Rab-binding domain of OCRL1. *The EMBO journal* **30**, 1659-1670, doi:emboj201160 [pii]  
10.1038/emboj.2011.60 (2011).
- 58 Choi, S. W., Gerencser, A. A. & Nicholls, D. G. Bioenergetic analysis of isolated cerebrocortical nerve terminals on a microgram scale: spare respiratory capacity and stochastic mitochondrial failure. *J Neurochem* **109**, 1179-1191, doi:JNC6055 [pii]  
10.1111/j.1471-4159.2009.06055.x (2009).
- 59 Jung, Y. S. & Zweckstetter, M. Mars -- robust automatic backbone assignment of proteins. *J Biomol NMR* **30**, 11-23 (2004).
- 60 Jung, Y. S. & Zweckstetter, M. Backbone assignment of proteins with known structure using residual dipolar couplings. *J Biomol NMR* **30**, 25-35 (2004).
- 61 Steinert, J. R. *et al.* Rab11 rescues synaptic dysfunction and behavioural deficits in a *Drosophila* model of Huntington's disease. *Human molecular genetics* **21**, 2912-2922, doi:10.1093/hmg/dds117 (2012).
- 62 Ali, Y. O., Escala, W., Ruan, K. & Zhai, R. G. Assaying locomotor, learning, and memory deficits in *Drosophila* models of neurodegeneration. *J Vis Exp*, doi:2504 [pii]  
10.3791/2504 (2011).
- 63 Craik, D. J. & Wilce, J. A. Studies of protein-ligand interactions by NMR. *Methods Mol Biol* **60**, 195-232 (1997).
- 64 Itzen, A. & Goody, R. S. GTPases involved in vesicular trafficking: structures and mechanisms. *Seminars in cell & developmental biology* **22**, 48-56 (2011).
- 65 Anderson, J. P. *et al.* Phosphorylation of Ser-129 is the dominant pathological modification of alpha-synuclein in familial and sporadic Lewy body disease. *J Biol Chem* **281**, 29739-29752, doi:M600933200 [pii]

10.1074/jbc.M600933200 (2006).

66 McLean, P. J., Kawamata, H. & Hyman, B. T. Alpha-synuclein-enhanced green fluorescent protein fusion proteins form proteasome sensitive inclusions in primary neurons. *Neuroscience* **104**, 901-912, doi:S0306-4522(01)00113-0 [pii] (2001).

67 Olzscha, H. *et al.* Amyloid-like aggregates sequester numerous metastable proteins with essential cellular functions. *Cell* **144**, 67-78, doi:10.1016/j.cell.2010.11.050 (2011).

68 Feany, M. B. & Bender, W. W. A Drosophila model of Parkinson's disease. *Nature* **404**, 394-398, doi:10.1038/35006074 35006074 [pii] (2000).

69 Pienaar, I. S., Gotz, J. & Feany, M. B. Parkinson's disease: insights from non-traditional model organisms. *Prog Neurobiol* **92**, 558-571, doi:S0301-0082(10)00159-0 [pii]

10.1016/j.pneurobio.2010.09.001 (2010).

70 Gajula Balija, M. B., Griesinger, C., Herzig, A., Zweckstetter, M. & Jackle, H. Pre-fibrillar alpha-synuclein mutants cause Parkinson's disease-like non-motor symptoms in Drosophila. *PLoS one* **6**, e24701, doi:10.1371/journal.pone.0024701

PONE-D-11-06498 [pii] (2011).

71 Nowicki, S., Jr. & Oxenford, C. The relation of hostile nonverbal communication styles to popularity in preadolescent children. *J Genet Psychol* **150**, 39-43, doi:10.1080/00221325.1989.9914572 (1989).

72 Sung, J. Y. *et al.* Induction of neuronal cell death by Rab5A-dependent endocytosis of alpha-synuclein. *J Biol Chem* **276**, 27441-27448, doi:10.1074/jbc.M101318200

M101318200 [pii] (2001).

73 Soper, J. H. *et al.* Alpha-synuclein-induced aggregation of cytoplasmic vesicles in *Saccharomyces cerevisiae*. *Mol Biol Cell* **19**, 1093-1103, doi:E07-08-0827 [pii]

10.1091/mbc.E07-08-0827 (2008).

74 Dalfo, E. & Ferrer, I. Alpha-synuclein binding to rab3a in multiple system atrophy. *Neurosci Lett* **380**, 170-175, doi:S0304-3940(05)00073-X [pii]

10.1016/j.neulet.2005.01.034 (2005).

75 Nakamura, S., Kawamoto, Y., Nakano, S. & Akiguchi, I. Expression of the endocytosis regulatory proteins Rab5 and Rabaptin-5 in glial cytoplasmic inclusions from brains with multiple system atrophy. *Clin Neuropathol* **19**, 51-56 (2000).

76 Henry, L. & Sheff, D. R. Rab8 regulates basolateral secretory, but not recycling, traffic at the recycling endosome. *Mol Biol Cell* **19**, 2059-2068, doi:E07-09-0902 [pii]

10.1091/mbc.E07-09-0902 (2008).

77 Rendon, W. O., Martinez-Alonso, E., Tomas, M., Martinez-Martinez, N. & Martinez-Menarguez, J. A. Golgi fragmentation is Rab and SNARE dependent in cellular models of Parkinson's disease. *Histochemistry and cell biology* **139**, 671-684, doi:10.1007/s00418-012-1059-4 (2013).

78 Lee, M. T., Mishra, A. & Lambright, D. G. Structural mechanisms for regulation of membrane traffic by rab GTPases. *Traffic (Copenhagen, Denmark)* **10**, 1377-1389 (2009).

79 Hutagalung, A. H., Coleman, J., Pypaert, M. & Novick, P. J. An internal domain of Exo70p is required for actin-independent localization and mediates assembly of specific exocyst components. *Mol Biol Cell* **20**, 153-163, doi:E08-02-0157 [pii]

10.1091/mbc.E08-02-0157 (2009).

80 Colla, E. *et al.* Accumulation of toxic alpha-synuclein oligomer within endoplasmic reticulum occurs in alpha-synucleinopathy in vivo. *J Neurosci* **32**, 3301-3305, doi:32/10/3301 [pii]

10.1523/JNEUROSCI.5368-11.2012 (2012).

81 Chesselet, M. F. In vivo alpha-synuclein overexpression in rodents: a useful model of Parkinson's disease? *Exp Neurol* **209**, 22-27, doi:S0014-4886(07)00307-X [pii]

10.1016/j.expneurol.2007.08.006 (2008).

82 El-Agnaf, O. M. *et al.* Aggregates from mutant and wild-type alpha-synuclein proteins and NAC peptide induce apoptotic cell death in human neuroblastoma cells by formation of beta-sheet and amyloid-like filaments. *FEBS letters* **440**, 71-75 (1998).

83 Tanik, S. A., Schultheiss, C. E., Volpicelli-Daley, L. A., Brunden, K. R. & Lee, V. M. Lewy body-like alpha-synuclein aggregates resist degradation and impair macroautophagy. *J Biol Chem* **288**, 15194-15210, doi:10.1074/jbc.M113.457408 (2013).

84 Forno, L. S. Neuropathology of Parkinson's disease. *J Neuropathol Exp Neurol* **55**, 259-272 (1996).

85 Jensen, P. H. *et al.* alpha-synuclein binds to Tau and stimulates the protein kinase A-catalyzed tau phosphorylation of serine residues 262 and 356. *J Biol Chem* **274**, 25481-25489 (1999).

86 Kawamata, H., McLean, P. J., Sharma, N. & Hyman, B. T. Interaction of alpha-synuclein and synphilin-1: effect of Parkinson's disease-associated mutations. *J Neurochem* **77**, 929-934 (2001).

87 De Genst, E. J. *et al.* Structure and properties of a complex of alpha-synuclein and a single-domain camelid antibody. *Journal of molecular biology* **402**, 326-343, doi:S0022-2836(10)00742-4 [pii]

10.1016/j.jmb.2010.07.001 (2010).

- 88 Burre, J. *et al.* Alpha-synuclein promotes SNARE-complex assembly in vivo and in vitro. *Science* **329**, 1663-1667, doi:10.1126/science.1195227 (2010).
- 89 Yap, T. L. *et al.* Alpha-synuclein interacts with Glucocerebrosidase providing a molecular link between Parkinson and Gaucher diseases. *J Biol Chem* **286**, 28080-28088, doi:M111.237859 [pii] 10.1074/jbc.M111.237859 (2011).
- 90 Jensen, P. H. *et al.* Microtubule-associated protein 1B is a component of cortical Lewy bodies and binds alpha-synuclein filaments. *J Biol Chem* **275**, 21500-21507, doi:10.1074/jbc.M000099200 M000099200 [pii] (2000).
- 91 Waxman, E. A. & Giasson, B. I. Characterization of kinases involved in the phosphorylation of aggregated alpha-synuclein. *J Neurosci Res* **89**, 231-247, doi:10.1002/jnr.22537 (2010).
- 92 Inglis, K. J. *et al.* Polo-like kinase 2 (PLK2) phosphorylates alpha-synuclein at serine 129 in central nervous system. *J Biol Chem* **284**, 2598-2602, doi:C800206200 [pii] 10.1074/jbc.C800206200 (2009).
- 93 Basso, E. *et al.* PLK2 Modulates alpha-Synuclein Aggregation in Yeast and Mammalian Cells. *Mol Neurobiol*, doi:10.1007/s12035-013-8473-z (2013).
- 94 Kuwahara, T., Tonegawa, R., Ito, G., Mitani, S. & Iwatsubo, T. Phosphorylation of alpha-synuclein protein at Ser-129 reduces neuronal dysfunction by lowering its membrane binding property in *Caenorhabditis elegans*. *J Biol Chem* **287**, 7098-7109, doi:10.1074/jbc.M111.237131 (2012).
- 95 Oueslati, A., Schneider, B. L., Aebischer, P. & Lashuel, H. A. Polo-like kinase 2 regulates selective autophagic alpha-synuclein clearance and suppresses its toxicity in vivo. *Proc Natl Acad Sci U S A* **110**, E3945-3954, doi:10.1073/pnas.1309991110 (2013).
- 96 Chen, L. & Feany, M. B. Alpha-synuclein phosphorylation controls neurotoxicity and inclusion formation in a *Drosophila* model of Parkinson disease. *Nat Neurosci* **8**, 657-663, doi:10.1038/nn1443 (2005).
- 97 Sato, H. *et al.* Authentically phosphorylated alpha-synuclein at Ser129 accelerates neurodegeneration in a rat model of familial Parkinson's disease. *J Neurosci* **31**, 16884-16894, doi:10.1523/JNEUROSCI.3967-11.2011 (2011).
- 98 McFarland, N. R. *et al.* Alpha-synuclein S129 phosphorylation mutants do not alter nigrostriatal toxicity in a rat model of Parkinson disease. *J Neuropathol Exp Neurol* **68**, 515-524, doi:10.1097/NEN.0b013e3181a24b53 (2009).
- 99 McFarland, M. A., Ellis, C. E., Markey, S. P. & Nussbaum, R. L. Proteomics analysis identifies phosphorylation-dependent alpha-synuclein protein interactions. *Mol Cell Proteomics* **7**, 2123-2137, doi:M800116-MCP200 [pii]

10.1074/mcp.M800116-MCP200 (2008).

- 100 Sancenon, V. *et al.* Suppression of alpha-synuclein toxicity and vesicle trafficking defects by phosphorylation at S129 in yeast depends on genetic context. *Hum Mol Genet* **21**, 2432-2449 (2012).
- 101 London, N., Raveh, B., Cohen, E., Fathi, G. & Schueler-Furman, O. Rosetta FlexPepDock web server--high resolution modeling of peptide-protein interactions. *Nucleic acids research* **39**, W249-253, doi:10.1093/nar/gkr431 (2011).
- 102 Raveh, B., London, N. & Schueler-Furman, O. Sub-angstrom modeling of complexes between flexible peptides and globular proteins. *Proteins* **78**, 2029-2040, doi:10.1002/prot.22716 (2010).
- 103 Baker, N. A., Sept, D., Joseph, S., Holst, M. J. & McCammon, J. A. Electrostatics of nanosystems: application to microtubules and the ribosome. *Proc Natl Acad Sci U S A* **98**, 10037-10041, doi:10.1073/pnas.181342398 (2001).

## Figure Legends

**Figure 1.**  $\alpha$ S interacts with endogenous Rab8a in rodent brain.  $\alpha$ S was immunoprecipitated (IP) from rat hippocampus or mouse cortical synaptosomes (**A**), and  $\alpha$ S and Rab8a were detected (IB). To further prove the interaction between the two proteins, Rab8a was immunoprecipitated from mouse cortical synaptosomes (**B**), and  $\alpha$ S and Rab8a were detected. Complete immunoblots are shown to demonstrate the specificity of the interaction.

**Figure 2.** Rab8a binds to the C-terminus of  $\alpha$ S. Averaged NMR chemical shift perturbation of  $^1\text{H}/^{15}\text{N}$  resonances of  $\alpha$ S in the presence of Rab8a(GDP) (**A**) and Rab8a(GppNHp) for molar ratios up to 1:10 and 1:8 respectively of  $\alpha$ S/Rab8a (**B**).

**Figure 3.**  $\alpha$ S binds to the nucleotide-binding region of Rab8a. (**A**)  $^1\text{H}-^{15}\text{N}$  HSQC spectrum of Rab8a(GDP). Selected sequence-specific resonance assignments are indicated. (**B**) Averaged NMR chemical shift perturbation of  $^1\text{H}/^{15}\text{N}$  resonances of Rab8a(GDP) in the presence of  $\alpha$ S. The Rab8a(GDP): $\alpha$ S molar ratio was 1:8. Secondary structure elements in the 3D structure of Rab8a(9-178)(GppNHp) (PDB code: 3QBT) are depicted above with blue and red boxes representing  $\beta$ -strands and  $\alpha$ -helices, respectively. (**C**) Residue-specific NMR signal intensity ratios in  $^1\text{H}-^{15}\text{N}$  HSQC of Rab8a(GDP) in the presence and absence of  $\alpha$ S. (**D**)  $\alpha$ S binding mapped onto the 3D structure of Rab8a(9-178)(GppNHp) (PDB code: 3QBT). Residues I<sup>43</sup>G<sup>44</sup>I<sup>45</sup>D<sup>46</sup> and T<sup>76</sup>Y<sup>79</sup>, for which the chemical shift perturbation shown in (B) exceeds 0.01 ppm and peak intensity ratios shown in (C) exceed 1.1, were colored pink. The NMR-invisible part of the switch II region is shown in blue, while the beginning of the C-terminal tail is colored red.  $\beta$ -strand  $\beta$ 3 that is part of the inter-Switch region is marked. (**E**) The C-terminus of  $\alpha$ S binds to the positively charged surface of Rab8a. A docking model of the complex of the  $\alpha$ S C-terminal peptide Y<sup>125</sup>-E<sup>137</sup> (shown in pink) with Rab8a was obtained using the Rosetta FlexPepDock web server<sup>101,102</sup>. S129 in the peptide was replaced by aspartic acid (D129 shown in yellow) to mimic the effect of phosphorylation. The electrostatic potential was calculated using the program APBS<sup>103</sup> on the basis of the 3D structure of Rab8a(9-178)(GppNHp) (PDB code: 3QBT).

**Figure 4.** Phosphorylation at S129 tightens the  $\alpha$ S-Rab8a interaction. **(A)** Primary sequence of the C-terminus of  $\alpha$ S. Residues of pS129  $\alpha$ S for which NMR signals were strongly broadened ( $I/I_0 < 0.4$  in C) are shown in purple. **(B)** Superposition of  $^1\text{H}$ - $^{15}\text{N}$  HSQC spectra of pS129 $\alpha$ S in the absence (green color) and presence (red color) of Rab8a(GDP) (1:5 molar ratio of  $\alpha$ S to Rab8a(GDP)). **(C)** Residue-specific NMR signal intensity ratios in  $^1\text{H}$ - $^{15}\text{N}$  HSQC spectra of different  $\alpha$ S variants in the presence and absence of Rab8a(GDP) ( $\square$ :Rab8a(GDP) molar ratio of 1:5). Data for wild-type, S129D and pS129  $\alpha$ S are shown in blue, green and red, respectively.

**Figure 5.** Rab8a enhances  $\alpha$ S fibrillization. **(A)** ThT fluorescence aggregation assay of  $\alpha$ S at different molar ratios of  $\alpha$ S:Rab8a(GDP). Error bars were estimated based on triplicate experiments. **(B-D)** Electron micrographs of samples taken after 90 hours of aggregation as shown in A). Images for the  $\alpha$ S control (B), and at molar ratios of 1:0.5 (C) and 1:1 (D).

**Figure 6.** Rab8a modulates  $\alpha$ S aggregation in cells. **(A)** Representative images of different categories: “No aggregates”, “less than 10 aggregates” and “10 or more aggregates”. **(B)** Rab8a increases the total number of cells with aggregates when compared to the control. **(C)** The presence of the phosphomimetic variant S129D  $\alpha$ S increases the number of aggregates per cell but not the total percentage of cells with aggregates whereas the S129A  $\alpha$ S mutant showed a reduction in the percentage of cells with inclusions. **(D)**  $\alpha$ S were positively-stained with NIAD-4, a dye that recognizes beta-amyloid structure. Scale bar: 5  $\mu\text{m}$ .

**Figure 7.** Rab8a rescues  $\alpha$ S -induced cellular toxicity. **(A)** Expression of  $\alpha$ S increases toxicity more than two-fold and is rescued by coexpression of Rab8a. All data are relative to total cell death and were normalized to empty vector control and represent data are mean  $\pm$  S.D. two-tailed paired t-test. **(B)** Protein expression levels remain unchanged in experimental conditions.  $\beta$ -Actin served as a loading control (immunoblots representative from 3 independent experiments are shown).

**Figure 8.** Rab8 rescues  $\alpha$ S-dependent crawling defects in *Drosophila* larvae.  $\alpha$ S expression in motoneurons **(A, C)** and dopaminergic neurons **(B, D)** decreases the distance covered by third instar larvae over a two minute interval. The

overexpression of Rab8 in either tissue rescues the crawling phenotype due to expression of the  $\alpha$ S variants (wild-type and TP mutant). N = 40 for each genotype analysed. Data are mean  $\pm$  S.E.M. ANOVA with *post hoc* tests. \* P < 0.05, \*\* P < 0.01, \*\*\* P < 0.001.

**Figure 9.** Pan-neuronal expression of Rab8 rescues  $\alpha$ S locomotor impairments. Expression of  $\alpha$ S via *elav* GAL4 significantly reduces climbing activity of adult fruit flies at day 10 post-eclosion, which is rescued by overexpression of Rab8. GFP +  $\alpha$ S flies served as controls for possible titration effects. N = 60 for each genotype analysed. Data are mean  $\pm$  S.E.M. ANOVA with *post hoc* tests. n.s. = not significant, \*\*\* P < 0.001.

**Figure 10.** Rab8 rescues the loss of dopaminergic neurons in *Drosophila*.  $\alpha$ S expression in the CNS (*elav*GAL4, upper panels) and in the dopaminergic neurons (*ple*GAL4, lower panels) significantly reduces the number of neurons in different dopaminergic clusters in day 30 adult fruit flies. The co-expression of Rab8 ameliorates this neurodegeneration. N = 16-34 brain hemispheres per genotype. Data are mean  $\pm$  S.E.M. ANOVA with *post hoc* tests. n.s. = not significant, \* p < 0.05, \*\* p < 0.01 and \*\*\* p < 0.001.

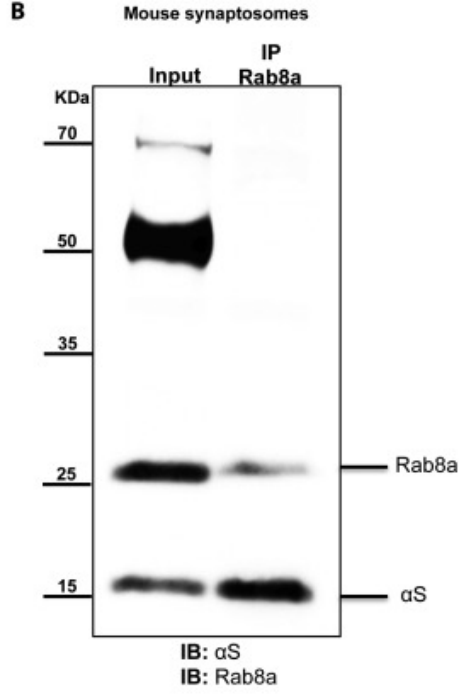
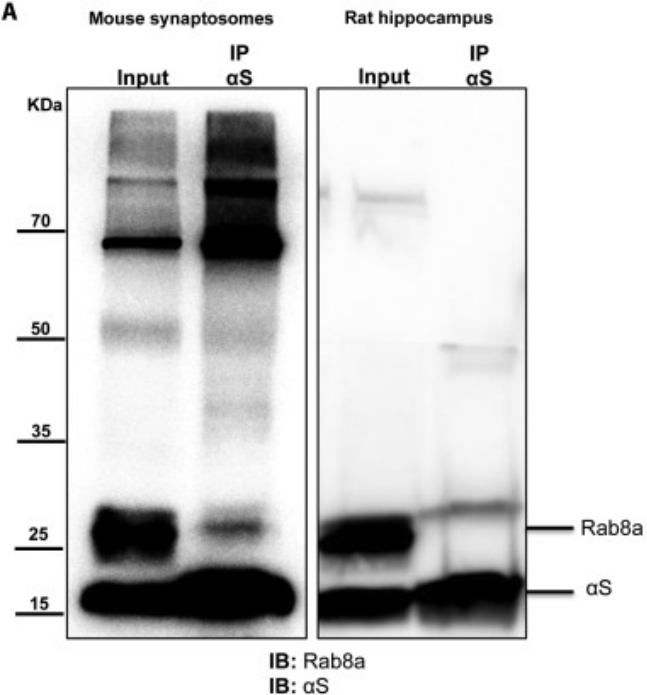
**Supplementary Figure S1.** Immunoprecipitation control. Total protein extracts from rat hippocampus were incubated with either a rabbit anti- $\alpha$ S antibody or with rabbit pre-immune serum as a control<sup>88</sup>. WB for Rab8a showed no signal in the control lane, validating the specificity of the interaction.

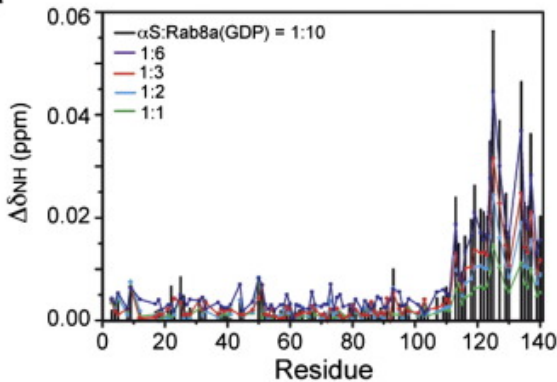
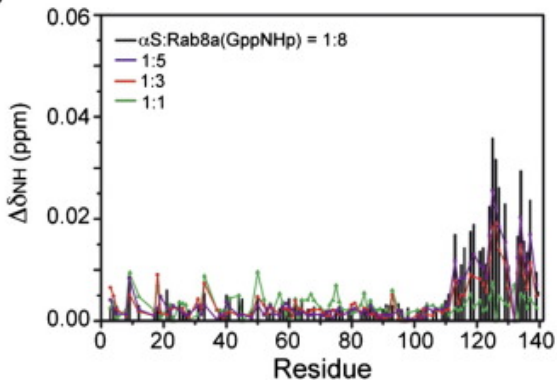
**Supplementary Figure S2.** Interaction of  $\alpha$ S with the C-terminally truncated variant Rab8a- $\delta$ C. Changes in cross-peak positions in two-dimensional HSQC spectra of  $\alpha$ S(GDP) (A) and Rab8a- $\delta$ C(GppNHp) (B) for molar ratios up to 1:10 of  $\alpha$ S/Rab8a- $\delta$ C. (C) NMR chemical shift perturbation of <sup>1</sup>H/<sup>15</sup>N resonances of Rab8a- $\delta$ C(GDP) upon addition of a peptide comprising residues 113-140 of  $\alpha$ S with S129 phosphorylated. The Rab8a- $\delta$ C(GDP):peptide molar ratio was 1:10.

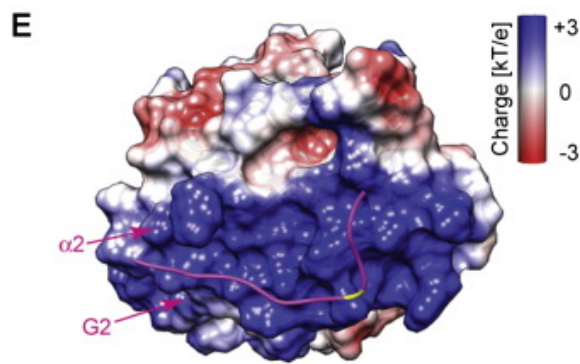
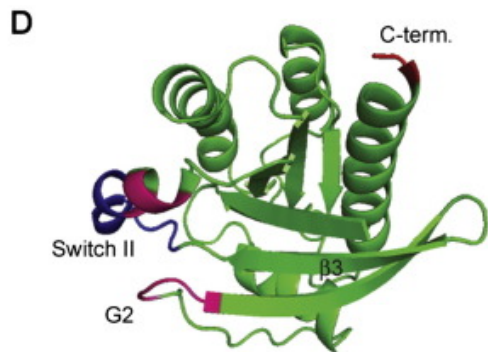
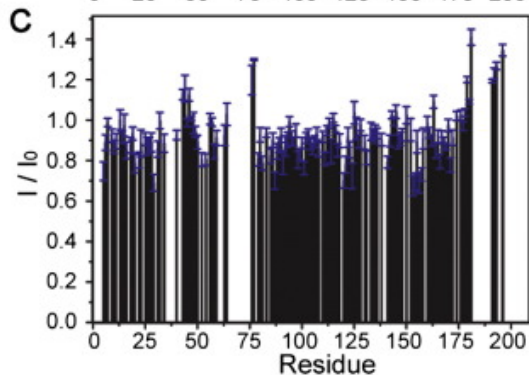
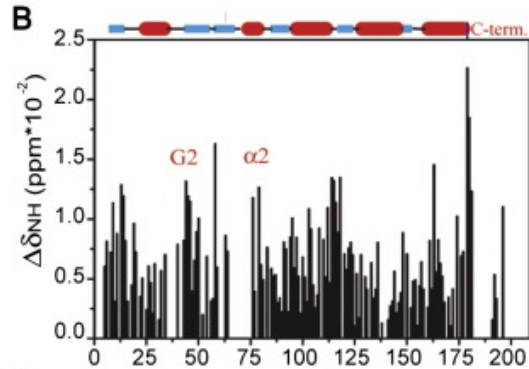
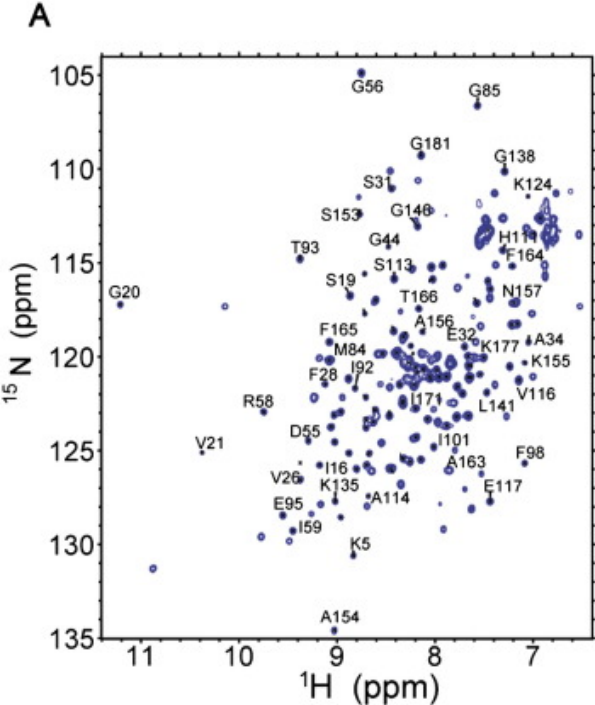
**Supplementary Figure S3.** ThT fluorescence intensity upon incubation of pure Rab8a(GDP) under the same conditions as used for co-incubation of Rab8a(GDP) and  $\alpha$ S.

**Supplementary Figure S4.** Endogenous (A) and overexpressed GFP-Rab8a (B) colocalize with  $\alpha$ S inclusions in cells.

Scale bar 10 m.

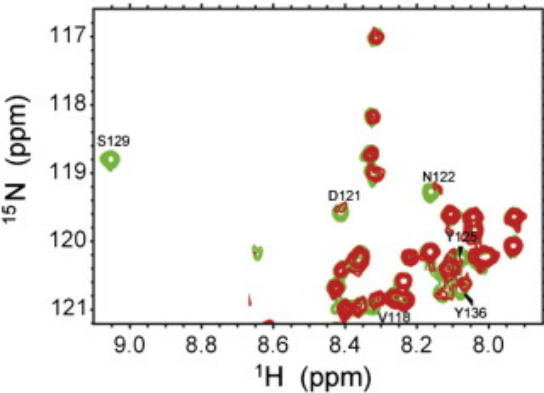
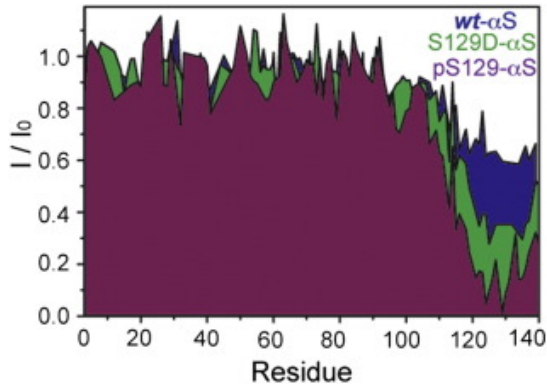


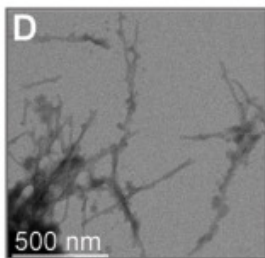
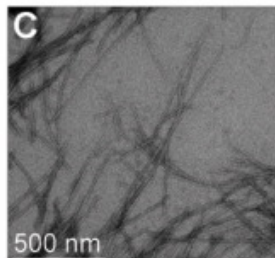
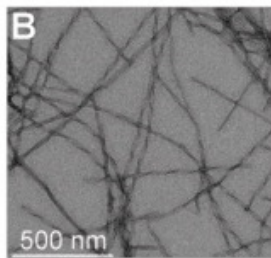
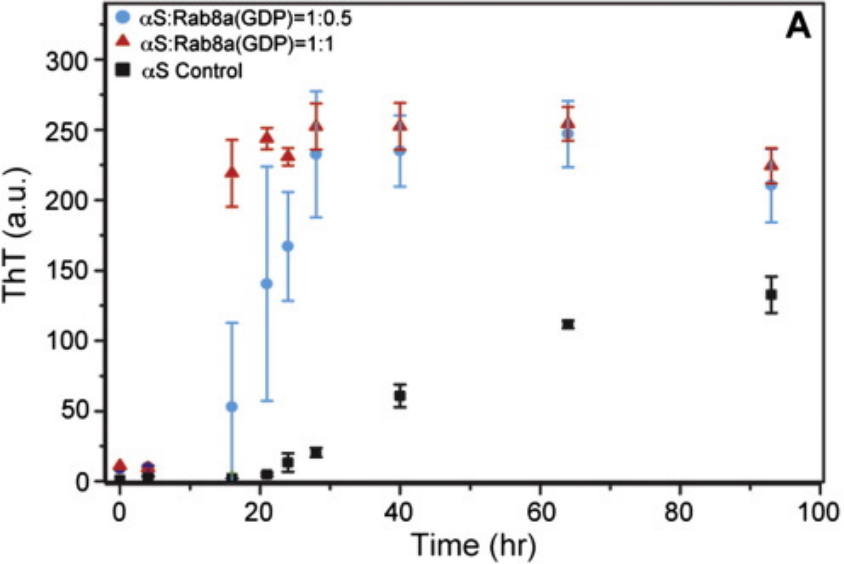
**A****B**

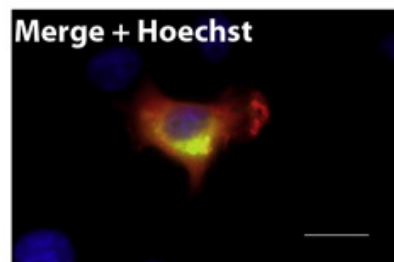
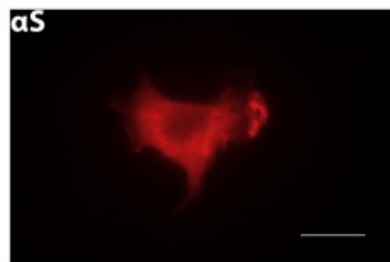
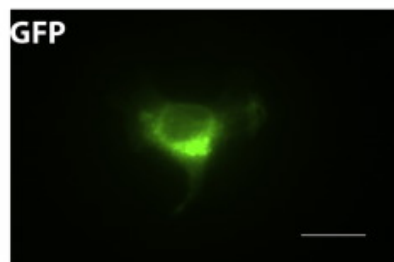
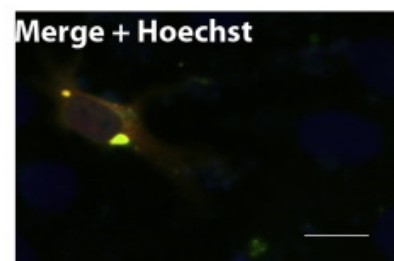
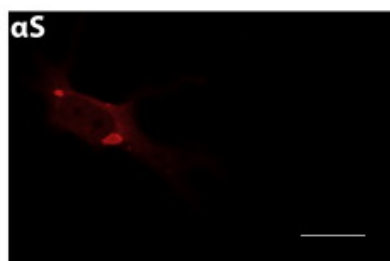
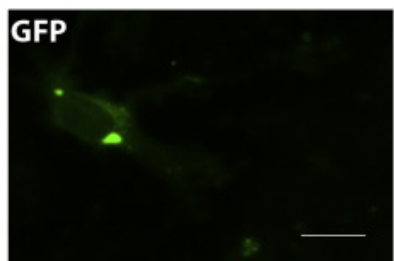
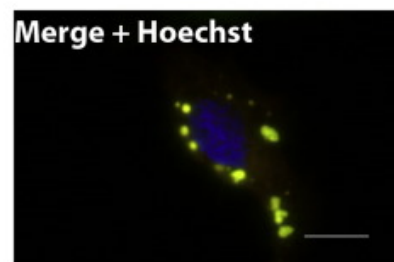
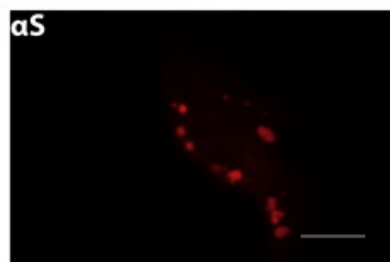
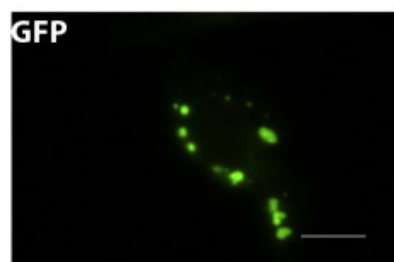
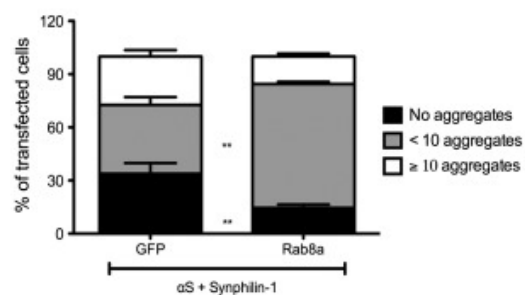
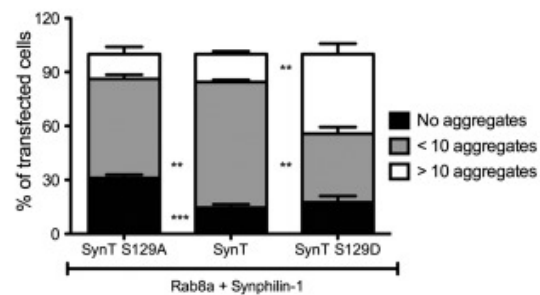
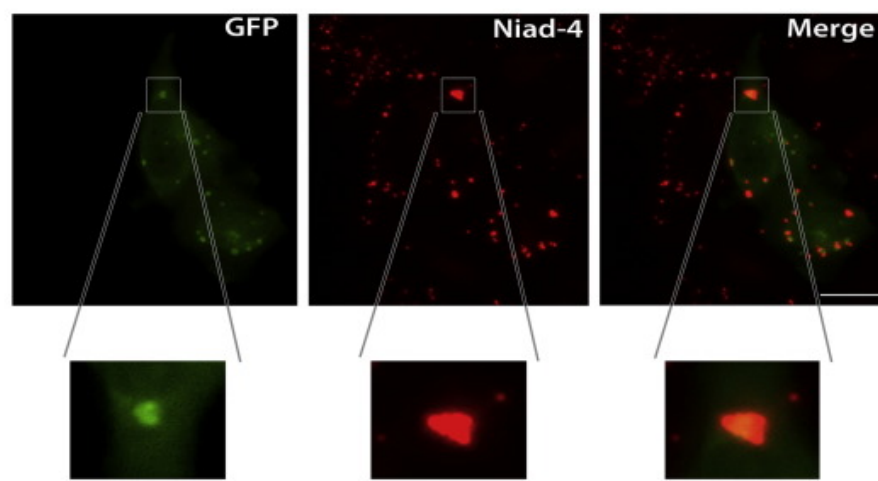


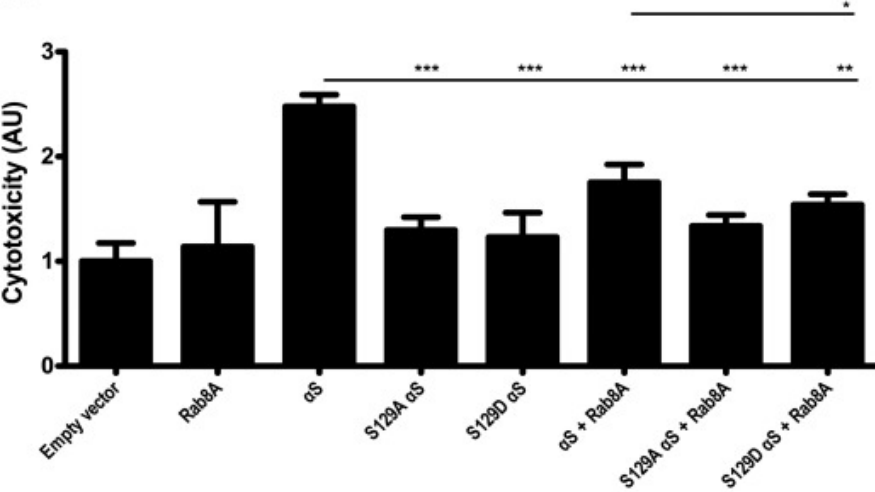
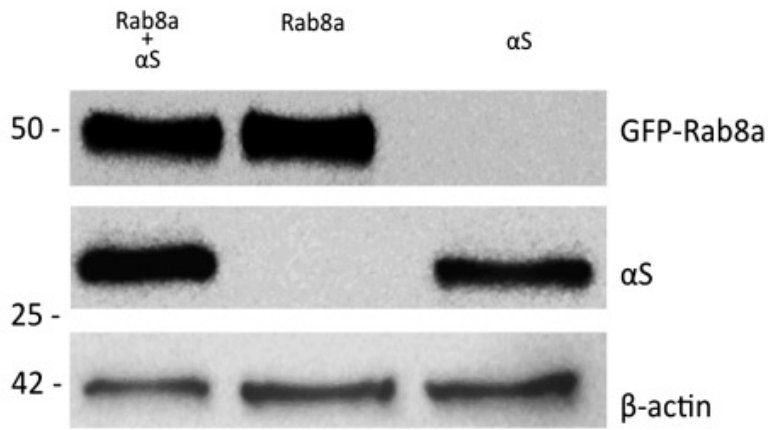
**A**

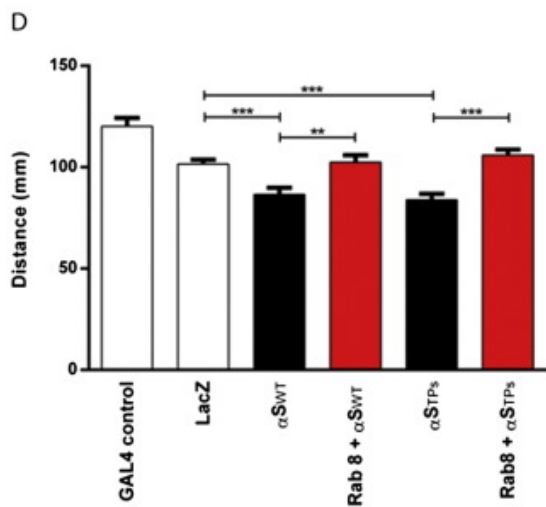
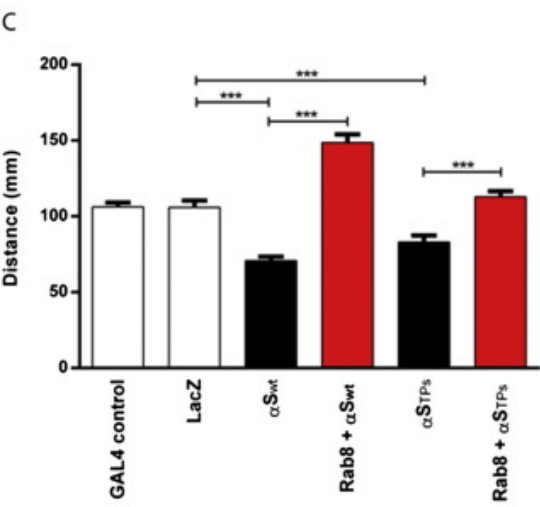
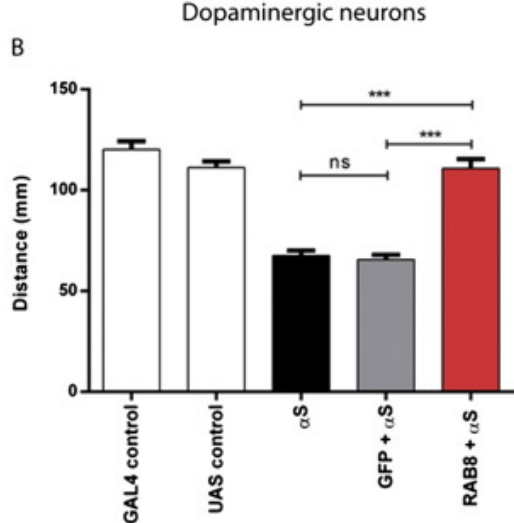
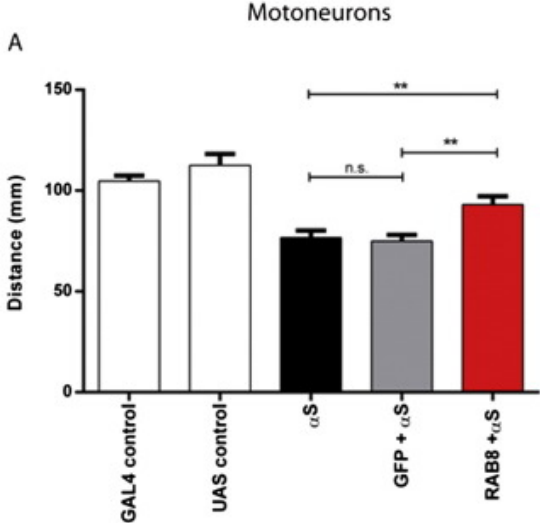
$\alpha$ S: L<sup>100</sup>GKNEEGAPQE<sup>110</sup>GILEDMPVDP<sup>120</sup>DNEAYEMPSE<sup>130</sup>EGYQDYPEA<sup>140</sup>

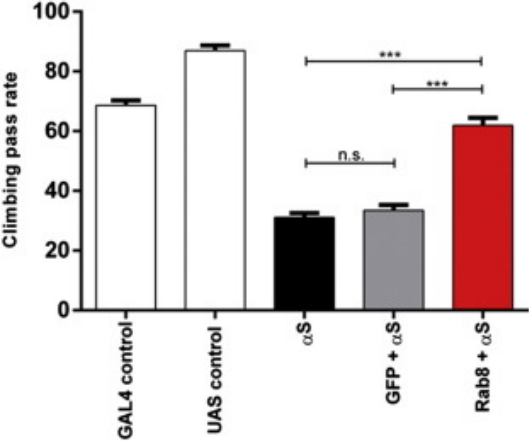
**B****C**



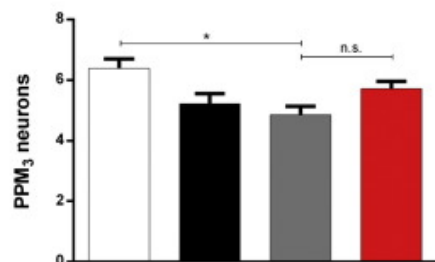
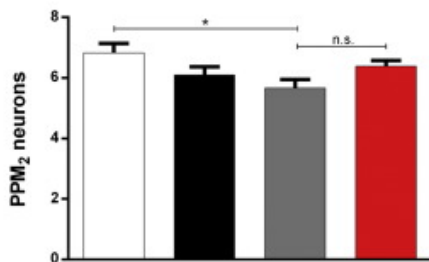
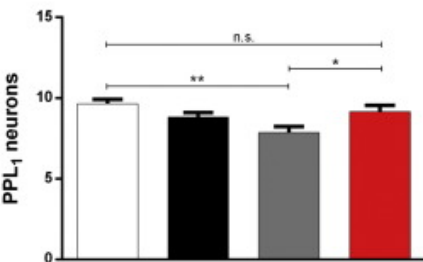
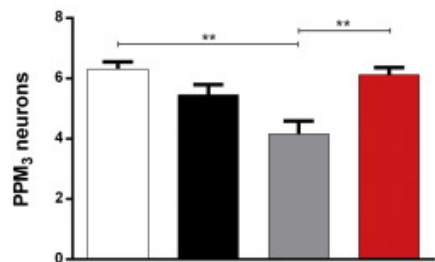
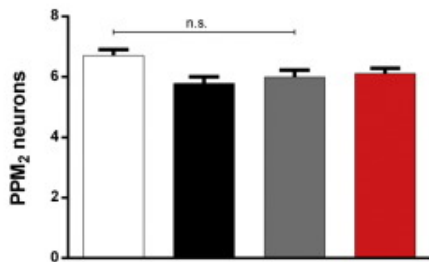
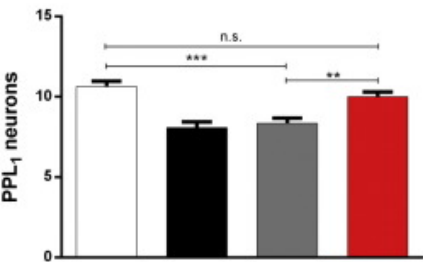
**A****No aggregates****< 10****≥ 10****B****C****D**

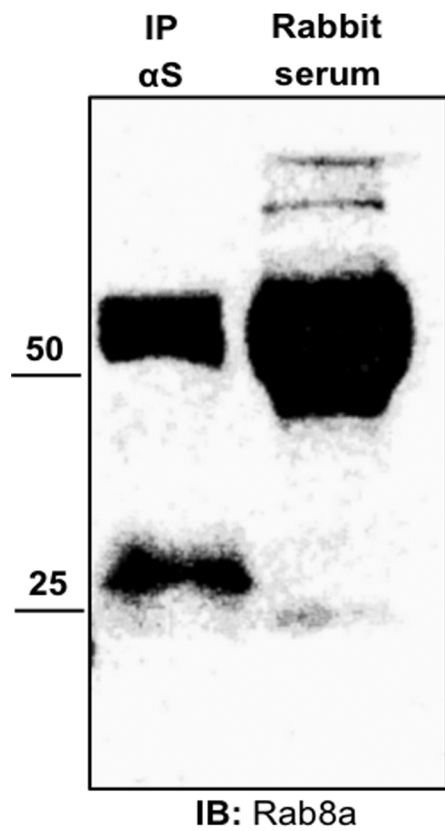
**A****B**

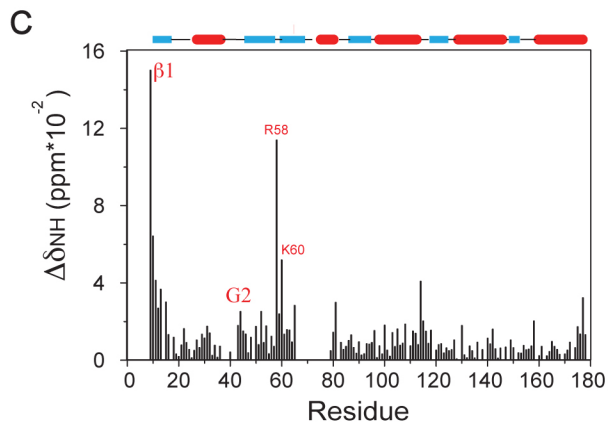
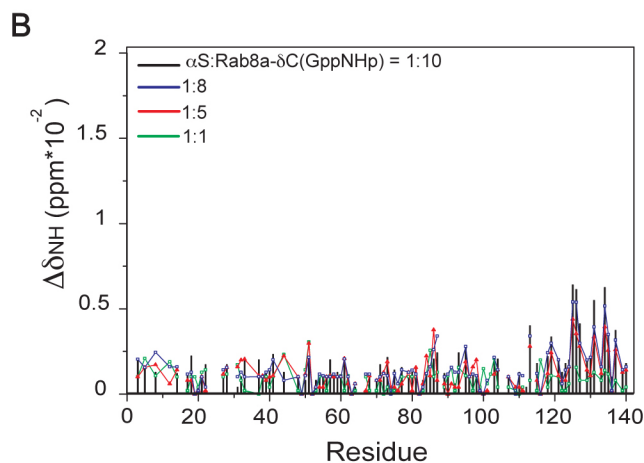
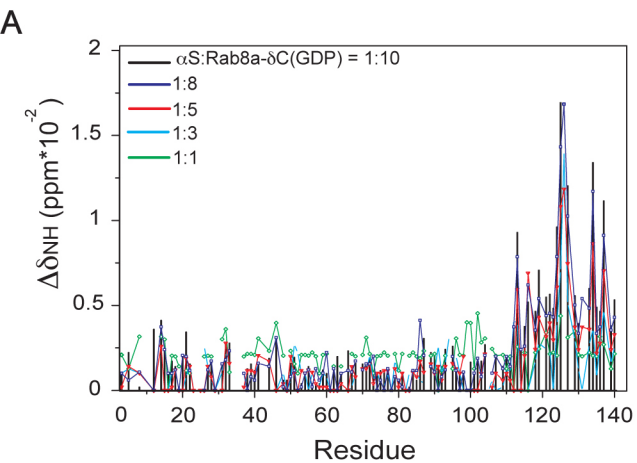


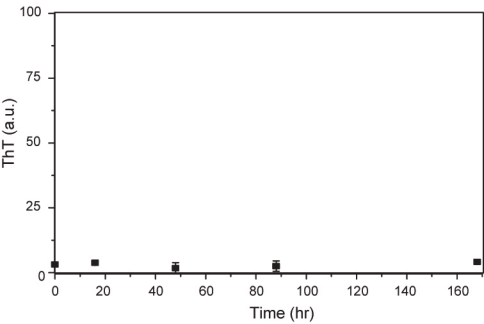


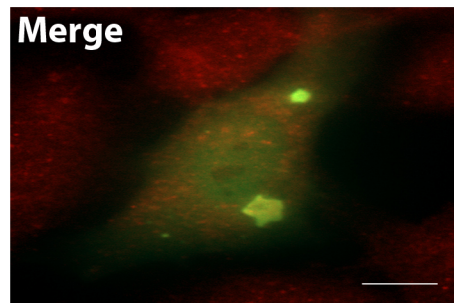
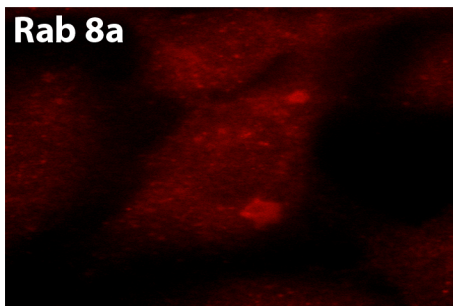
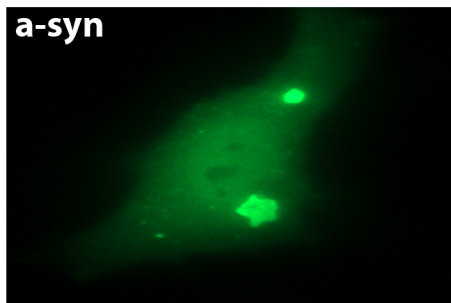
□ Driver control    ■  $\alpha S_{WT}$     ■ GFP +  $\alpha S_{WT}$     ■ Rab8 +  $\alpha S_{WT}$









**A****B**